effects were primarily due to suppressed bone turnover. On the other hand, Cal treatment attenuated the GC-induced decrease in cancellous BV/TV and Tb Th. These effects were primarily due to suppressed bone resorption and maintained or even increased bone formation. Thus, the differential effects of Ris and Cal on cancellous osteopenia were shown in GC-treated rats.

As discussed above, increased bone resorption and suppressed bone formation contributes to GC-induced bone loss. In addition, suppression of intestinal calcium absorption and decreased renal tubular calcium reabsorption with increased urinary calcium excretion have also been reported to contribute partly to GC-induced bone loss [7]. In our study, renal and intestinal calcium losses were not evaluated; however GC administration decreased serum calcium levels, suggesting that it might also suppress intestinal calcium absorption and renal tubular calcium reabsorption. Ris treatment accelerated the GC-induced decrease in serum calcium levels, probably because of accumulation in the bone of calcium from serum. However, Cal failed to increase serum calcium levels. Higher doses of Cal and/or much more calcium supplementation might be needed for serum calcium levels to increase.

Ris treatment prevented GC-induced deceases in longitudinal bone growth and tibial length. This result suggests that Ris does not adversely affect longitudinal bone growth in rats treated with GC. However, Cal treatment did not show any effect on tibial length, as previously reported [10].

Limitations should be noted. The duration of the study (4 weeks) seems to be too short. However, evidence suggests that the loss of BMD is more evident in cancellous bone than in cortical bone [23], and that high-dose GC therapy induces the rapid loss of BMD [24]. Actually, the present study did confirm that the high-dose GC administration induced cancellous osteopenia and deterioration of cancellous microarchitecture, as a result of increased bone resorption and decreased bone formation, and showed the differential effect of Ris and Cal on cancellous microarchitecture and bone formation and resorption in the early phase (4 weeks) of the high-dose GC administration. Further studies with longer duration of observation would be of interest to determine the effect of Ris and Cal on cortical bone as well as bone mechanical strength in GC-treated rats.

In conclusion, the present study showed the differential effects of Ris and Cal on cancellous osteopenia in rats treated with high-dose GC. The effects of Ris on cancellous osteopenia were associated with suppressed bone turnover, while those of Cal were associated with suppressed bone resorption and maintained or even increased bone formation.

References

1. Amin, S., Lavalley, M.P., Simms, R.W., and Felson, D.T. 2002. The comparative efficacy of drug therapies used for the management of corticosteroid-induced osteoporosis: a meta-regression. *J. Bone Miner. Res.* 17: 1512–1526.
2. Cranney, A., Wekch, V., Adachi, J.D., Homik, J., Shea, B., Suarez-Almazor, M.E., Tugwell, P., and Wells, G. 2000. Calcitonin for the treatment and prevention of corticosteroid-induced osteoporosis. *Cochrane Detabase Syst. Rev.* 2: CD001983.
3. Erben, R.G. 1997. Embedding of bone samples in methylmethacrylate: an improved method suitable for bone histomorphometry, histochemistry, and immunohistochemistry. *J. Histochem. Cytochem.* 45: 307–313.
4. Erben, R.G., Mosekilde, L., Thomsen, J.S., Weber, K., Stahr, K., Leyshon, A., Smith, S.Y., and Phipps, R. 2002. Prevention of bone loss in ovariectomized rats by combined treatment with risedronate and 1alpha,25-dihydroxyvitamin D_3. *J. Bone Miner. Res.* 17: 1498–1511.
5. Furuichi, H., Fukuyama, R., Izumo, N., Fujita, T., Kohno, T., Nakamuta, H., and Koida, M. 2000. Bone-anabolic effect of salmon calcitonin on glucocorticoid-induced osteopenia in rats. *Bio. Pharm. Bull.* 23: 946–951.
6. Hara, K., Kobatasi, M., and Akiyama, Y. 2002. Vitamin K_2 (menatetrenone) inhibits bone loss induced by prednisolone partly through enhancement of bone formation in rats. *Bone* 31: 575–581.
7. Hodgson, S.F. 1990. Corticosteroid-induced osteoporosis. *Endocrinol. Metab. Clin. North Am.* 19: 95–111.
8. Homik, J., Suarez-Almazor, M.E., Shea, B., Cranney, A., Wells, G., and Tugwell, P. 2000. Calcium and vitamin D for corticosteroid-induced osteoporosis. *Cochrane Database Syst. Rev.* 2: CD000952.
9. Homik, J., Cranney, A., Shea, B., Tugwell, P., Wells, G., Adachi, R., and Suarez-Almazor, M. 2000. Bisphosphonates for steroid induced osteoporosis. *Cochrane Database Syst. Rev.* 2: CD001347.
10. Jowell, P.S., Epstein, S., Fallon, M.D., Reinhardt, T.A., and Ismail, F. 1987. 1,25-dihydroxyvitamin D_3 modulates glucocorticoid-induced alteration in serum bone Gla protein and bone histomorphometry. *Endocrinology* 120: 531–536.
11. Lin, B.Y., Jee, W.S., Ma, Y.F., Ke, H.Z., Kimmel, D.B., and Li, X.J. 1994. Effects of prostaglandin E_2 and risedronate administration on cancellous bone in older female rats. *Bone* 15: 489–496.
12. Manolagas, S.C. and Weinstein, R.S. 1999. New

developments in the pathogenesis and treatment of steroid-induced osteoporosis. *J. Bone Miner. Res.* 14: 1061–1066.
13. Mosekilde, L., Thomsen, J.S., Mackey, M.S., and Phipps, R.J. 2000. Treatment with risedronate or alendronate prevents hind-limb immobilization-induced loss of bone density and strength in adult female rats. *Bone* 27: 639–645.
14. Nawata, H., Soen, S., Takayanagi, R., Tanaka, I., Takaoka, K., Fukunaga, M., Matsumoto, T., Suzuki, Y., Tanaka, H., Fujiwara, S., Miki, T., Sagawa, A., Nishizawa, Y., and Seino, Y. 2005. The subcommittee to study diagnostic criteria for glucocorticoid-induced osteoporosis. Guidelines on the management and treatment of glucocorticoid-induced osteoporosis of the Japanese Society for Bone and Mineral Research (2004). *J. Bone Miner. Metab.* 23: 105–109.
15. Noa, M., Mendoza, S., Mas, R., Mendoza, N., and Leon, F. 2004. Effect of D-003, a mixture of very high molecular weight aliphatic acids, on prednisolone-induced osteoporosis in Sprague-Dawley rats. *Drugs R. D.* 5: 281–290.
16. Nitta, T., Fukushima, T., Nakamuta, H., and Koida, M. 1999. Glucocorticoid-induced secondary osteopenia in female rats: a time course study as compared with ovariectomy-induced osteopenia and response to salmon calcitonin. *Jpn. J. Pharmacol.* 79: 379–386.
17. Ortoft, G. and Oxlund, H. 1996. Qualitative alterations of cortical bone in female rats after long-term administration of growth hormone and glucocorticoid. *Bone* 18: 581–590.
18. Otomo, H., Sakai, A., Ikeda, S., Tanaka, S., Ito, M., Phipps, R.J., and Nakamura, T. 2004. Regulation of mineral-to-matrix ratio of lumbar trabecular bone in ovariectomized rats treated with risedronate in combination with or without vitamin K_2. *J. Bone Miner. Metab.* 22: 404–414.
19. Parfitt, A.M., Drezner, M.K., Glorieux, F.H., Kanis, J.A., Malluche, H., Meunier, P.J., Ott, S.M., and Recker, R.R. 1987. Bone histomorphometry: standardization of nomenclature, symbols, and units. Report of the ASMBR Histomorphometry Nomenclature Committee. *J. Bone Miner. Res.* 2: 595–610.
20. Prakasam, G., Yeh, J.K., Chen, M.M., Castro-Magana, M., Liang, C.T., and Aloia, J.F. 1999. Effects of growth hormone and testosterone on cortical bone formation and bone density in aged orchiectomized rats. *Bone* 24: 491–497.
21. Richy, F., Ethgen, O., Bruyere, O., and Reginster, J.Y. 2004. Efficacy of alphacalcidol and calcitriol in primary and corticosteroid-induced osteoporosis: a meta-analysis of their effects on bone mineral density and fracture rate. *Osteoporos. Int.* 15: 301–310.
22. Tanaka, Y., Nakamura, T., Nishida, S., Suzuki, K., Takeda, S., Sato, K., and Nishii, Y. 1996. Effects of a synthetic vitamin D analog, ED-71, on bone dynamics and strength in cancellous and cortical bone in prednisolone-treated rats. *J. Bone Miner. Res.* 11: 325 –336.
23. Van Staa, T.P., Leufkens, H.G., Abenhaim, L., Zhang, B., and Cooper, C. 2000. Use of oral corticosteroids and risk of fractures. *J. Bone Miner. Res.* 15: 993–1000.
24. Van Staa, T.P., Leufkens, H.G., and Cooper, C. 2002. The epidemiology of corticosteroid-induced osteoporosis: a meta-analysis. *Osteoporos. Int.* 13: 777–787.

Exp. Anim. 55(4), 357–367, 2006

Comparative Effects of Alendronate and Alfacalcidol on Cancellous and Cortical Bone Mass and Bone Mechanical Properties in Ovariectomized Rats

Jun IWAMOTO[1], Azusa SEKI[2], Tsuyoshi TAKEDA[1], Yoshihiro SATO[3], Harumoto YAMADA[4], and James K. YEH[5]

[1] *Department of Sports Medicine, Keio University School of Medicine, 35 Shinanomachi, Shinjuku-ku, Tokyo 160-8582,* [2] *Hamri Co., Ltd., Tokyo,* [3] *Department of Neurology, Mitate Hospital, Fukuoka,* [4] *Department of Orthopaedic Surgery, Fujita Health University, Aichi, Japan and* [5] *Metabolism Laboratory, Department of Medicine, Winthrop-University Hospital, NY, USA*

Abstract: *The purpose of the present study was to compare the effects of alendronate and alfacalcidol on cancellous and cortical bone mass and bone mechanical properties in ovariectomized rats. Twenty-six female Sprague-Dawley rats, 7 months of age, were randomized by the stratified weight method into four groups: the sham-operated control (Sham) group and the three ovariectomy (OVX) groups, namely, OVX + vehicle, OVX + alendronate (2.5 mg/kg, p.o., daily), and OVX + alfacalcidol (0.5 μg/kg, p.o., daily). At the end of the 8-week experimental period, bone histomorphometric analyses of cancellous bone at the proximal tibial metaphysis and cortical bone at the tibial diaphysis were performed, and the mechanical properties of the femoral distal metaphysis and femoral diaphysis were evaluated. OVX decreased cancellous bone volume per total tissue volume (BV/TV), and the maximum load of the femoral distal metaphysis, as a result of increases in serum osteocalcin (OC) levels, and also the number of osteoclasts (N.Oc), osteoclast surface (OcS) and bone formation rate (BFR) per bone surface (BS), and BFR/BV, without any effect on cortical area (Ct Ar), or maximum load of the femoral diaphysis. Alendronate prevented this decrease in cancellous BV/TV by suppressing increases in N.Oc/BS, OcS/BS, BFR/BS, and BFR/BV, without any apparent effect on Ct Ar, or maximum load of the femoral distal metaphysis and femoral diaphysis. On the other hand, alfacalcidol increased cancellous BV/TV, Ct Ar, and the maximum load of the femoral distal metaphysis and femoral diaphysis, by mildly decreasing trabecular BFR/BV, maintaining trabecular mineral apposition rate and osteoblast surface per BS, increasing periosteal and endocortical BFR/BS, and preventing an increase in endocortical eroded surface per BS. The present study clearly showed the differential skeletal effects of alendronate and alfacalcidol in ovariectomized rats. Alendronate prevented OVX-induced cancellous bone loss by*

(Received 19 December 2005 / Accepted 8 March 2006)

Address corresponding: J. Iwamoto, Department of Sports Medicine, Keio University School of Medicine, 35 Shinanomachi, Shinjuku-ku, Tokyo 160-8582, Japan

suppressing bone turnover, while alfacalcidol improved cancellous and cortical bone mass and bone strength by suppressing bone resorption and maintaining or even increasing bone formation.

Key words: *alendronate, alfacalcidol, osteopenia, ovariectomy, rat*

Introduction

Alendronate (a bisphosphonate, anti-resorptive agent) and alfacalcidol (active vitamin D_3) are widely used for the treatment of postmenopausal osteoporosis in Japan. The results of randomized controlled head-to-head trials suggest that alendronate (5 mg/day) is more effective than alfacalcidol (1 μg/day) in increasing lumbar bone mineral density (BMD) and reducing the incidence of vertebral fractures in Japanese postmenopausal women with osteoporosis [14, 23]. However, their effects on BMD and the incidence of fractures of skeletal sites rich in cortical bone remain uncertain.

Several preclinical studies have reported the efficacy of alendronate and alfacalcidol against osteopenia using a rat model of postmenopausal women. Alendronate suppresses bone turnover and prevents cancellous bone loss, or even increases cancellous bone mass, in ovariectomized rats [6, 9, 20]. On the other hand, alfacalcidol suppresses bone resorption, yet maintains or even stimulates bone formation, as reflected by increases in serum osteocalcin levels and bone formation rate at both cancellous and cortical bone sites, thereby increasing BMD and improving the mechanical properties of the bone [21]. However, very few studies have reported on the comparative effects of alendronate and alfacalcidol on both the bone mass and mechanical properties of skeletal sites rich in cancellous or cortical bone in ovariectomized rats. The purpose of the present study was to compare the effects of alendronate and alfacalcidol on cancellous and cortical bone mass and bone mechanical properties in ovariectomized rats.

Materials and Methods

Treatment of animals

Twenty-six female Sprague-Dawley rats, 7 months of age, were purchased from Charles River Japan (Kanagawa, Japan). They were fed a pelleted standard chow diet containing 1.25% calcium and 0.9% phosphorus (CRF-1: Oriental Kobo, Co., Ltd., Tokyo, Japan). The animals were housed under local vivarium conditions (temperature 23.3°C, humidity 55%, and a 12-h on/off light cycle), with free access to water. After allowing one week for adaptation to the new environment, the rats were randomized by the stratified weight method into the following four groups: the sham-operation + vehicle (Sham) group (n=5), and the three bilateral ovariectomy (OVX) groups, namely, OVX + vehicle (n=5), OVX + alendronate (2.5 mg/kg, n=8), and OVX + alfacalcidol (0.5 μg/kg, n=8). The treatment with vehicle, alendronate, or alfacalcidol was started one day after the surgery and continued for 8 weeks. Bilateral OVX was performed under general anesthesia induced by intraperitoneal injection of 25–30 mg/kg pentobarbital sodium. Tablet forms of alendronate (Bonalon, Teijin Pharma, Tokyo, Japan) or alfacalcidol (One-alfa, Teijin Pharma, Tokyo, Japan) were pulverized, dissolved in 0.1 ml of sterile saline, and administered orally to the animals (the OVX + alendronate and OVX + alfacalcidol groups, respectively) every day by gavage deep into the mouth. Vehicle (0.1 ml of sterile saline) was also administered orally to the animals (the Sham + vehicle and OVX + vehicle groups) every day by gavage deep into the mouth. The dose of alendronate was determined based on the results of a previous study [1]. In OVX rats, 1.0 mg/kg of oral alendronate prevented OVX-induced cancellous bone loss in the proximal metaphysis, while 5.0 mg/kg of oral alendronate prevented OVX-induced BMD loss of the proximal femur. Thus, in the present study, 2.5 mg/kg of oral alendronate was adopted. The dose of alfacalcidol was determined so that the dose ratio of alfacalcidol to alendronate was 1 μg/5 mg based on the clinically available dose. This dose of alfacalcidol was considered to be effective, but was high according to the results of previous studies [10, 21, 22]. The body weight of the rats was monitored weekly. The present study was carried out at the laboratory of Hamri Co., Ltd. (Ibaraki, Japan). The animals

were maintained according to the National Institutes of Health (NIH) Guide for Care and Use of Laboratory Animals, and the animal experimental protocols were approved by the Laboratory Animal Care Committee of Hamri Co., Ltd. (Ibaraki, Japan).

Preparation of specimens

All the rats were labeled with 25 mg/kg tetracycline (Sigma Chemical, St. Louis, MO, USA) injected intramuscularly and 8 mg/kg calcein (Sigma Chemical, St. Louis, MO, USA) injected subcutaneously at 9 days and 3 days, respectively, before sacrifice. The rats were sacrificed at 8 weeks after the start of the experiment. Before the animals were sacrificed, urine samples were collected over a 24-h period using metabolic cages, and the specimens were stored at –20°C. The animals were sacrificed by exsanguination after being anesthetized by intraperitoneal injection of 25–30 mg/kg pentobarbital sodium. Serum specimens were collected from all the rats, and the right femur and right tibia were isolated.

The serum samples were stored at –20°C. The urine and serum samples were used for the measurements of the biochemical markers as described below. The femurs were stored at –20°C and then used for biomechanical testing as described below. The tibiae were processed for bone histomorphometric analyses. The bones were fixed in cold 40% ethanol overnight, and then cut into three parts using an Isomet saw (Buehler, Lake Bluff, IL, USA). The proximal tibial metaphysis and tibial diaphysis with the fibular junction were stained with Villanueva Osteochrome Bone Stain (Polyscience, Warrington, PA, USA) for 5 days. The specimens were dehydrated sequentially in ascending concentrations of ethanol (70%, 95%, and 100%) and xylene, and then embedded in methyl-methacrylate (EM Science, Gibbstown, NJ, USA) at 4°C according to the method of Erben [7]. Cross-sections of the tibial diaphysis just proximal to the tibio-fibular junction were cut at 40 μm thickness using a diamond wire Histo-Saw machine (Delaware Diamond Knives, Wilmington, DE, USA), and the thickness of each cross-sectional specimen was determined with an Inspectors' Dial Bench Gauge (L.S. Starrett, Athol, MA, USA). Frontal sections of the proximal tibial metaphysis were cut at 8 μm or 4 μm thickness using a microtome (Leica RM2155; Leica Inc., Nussloch, Germany). The 8-μm sections were then transferred onto chromalum-gelatin-coated slides and dried overnight under a press at 42°C. All the sections were coverslipped with Eukitt (Calibrated Instruments, Hawthorne, NY, USA) for the static and dynamic histomorphometric analyses. For tartrate-resistant acid phosphatase (TRAP) histochemistry, 8-μm sections of the proximal tibial metaphysis were deplasticized with three changes of 2-methoxyethylacetate for 30 min each, two changes of acetone for 5 min each, and sequential changes of ethanol (95%, 70%, and 40%), and finally, two changes of deionized water for 5 min each for rehydration. The deplasticized and rehydrated sections (8 μm thickness) were placed in 0.1 M acetate buffer at pH 5.0 for 5 min, and the TRAP reaction was subsequently performed using a leukocyte acid phosphatase kit (Sigma Chemical, St. Louis, MO, USA). The sections stained for TRAP were counterstained using Mayer's hematoxylin (1 min) and the sections were air-dried and mounted with a plastic UV mounting medium (Polysciences Inc., Warrington, PA, USA). For Goldner Trichrom staining to count the osteoblast surface, adjacent 4-μm sections of the proximal tibia metaphysis were deplasticized and rehydrated, followed by the procedure of Goldner Trichrom stain, then mounted with Eukitt (Calibrated Instruments, Hawthorne, NY, USA).

Urine and serum biochemical analyses

The levels of urinary deoxypyridinoline (DPD) as a bone resorption marker were measured by enzyme-immunoassay (EIA) using a Pyrilinks-D kit (Metra Biosystems Inc., CA, USA). The serum calcium and phosphorus levels were measured by the o-CPC and ammonium molybdate colorimetric methods, respectively, using an autoanalyzer (Dada Behring Model RXL, Bakersfield, CA, USA). The levels of serum osteocalcin (OC) as a bone formation marker were measured by immunoradiometric assay (IRMA) using a Rat Osteocalcin IRMA kit (Immutopics, Inc., CA, USA).

Biomechanical testing

The mechanical properties of the femoral diaphysis were evaluated by the three-point bending test. Load was applied midway between two supports placed 15 mm apart on the bone. The femur was positioned so that the loading point was at the center of the femoral diaphysis and bending occurred about the medial-lat-

eral axis. The specimens were tested in a saline bath at 37°C. Each specimen was submerged in the saline bath for about 3 min before the testing, to allow temperature equilibration. Load-displacement curves were recorded at a crosshead speed of 20 mm/min using a materials-testing machine (MZ500D; Maruto, Co., Ltd., Tokyo, Japan). The parameters analyzed were the maximum load, stiffness, and breaking energy.

Just after the three-point bending test of the femoral diaphysis, the distal metaphysis of the femur was isolated over a length of 10 mm from the joint surface of the femoral condyle. The mechanical properties of this segment were then measured by the compression test. Compressive load was applied by the rectangular parallelepiped crosshead (length 2 cm, width 2 cm, and height 1 cm) on the femoral distal metaphysis from the lateral aspect to the medial aspect. The specimens were positioned so that the loading point was at the center of the femoral lateral condyle. The specimens were tested in a saline bath at 37°C. Each specimen was submerged in the saline bath for about 3 min before the testing, to allow temperature equilibration. Load-displacement curves were recorded at a crosshead speed of 10 mm/minute and compression depth of 2.5 mm, using a materials-testing machine (MZ500D; Maruto, Co., Ltd., Tokyo, Japan). The parameters analyzed were maximum load, stiffness, and breaking energy.

Bone histomorphometry of the tibia

A digitizing morphometry system was used to measure bone histomorphometric parameters. The system consisted of an epifluorescence microscope (Nikon E-400, OsteoMetrics, Atlanta, GA, USA), an Osteomeasure High Resolution Color Subsystem (OsteoMetrics, Atlanta, GA, USA), and a digitizing pad (Numonics 2206; Numonics Corp., Montomerville, PA, USA) coupled to an IBM computer, and a morphometry program (OsteoMetrics, Atlanta, GA, USA). The measured parameters for cancellous bone included total tissue volume (TV), bone volume (BV), bone surface (BS), eroded surface (ES), single- and double-labeled surfaces (sLS and dLS, respectively), and osteoblast surface (ObS). These data were used to calculate percent cancellous bone volume (BV/TV), trabecular number (Tb N), trabecular thickness (Tb Th), trabecular separation (Tb Sp), ES/BS, MS/BS [(sLS/2+dLS)/BS], mineral apposition rate (MAR), bone formation rate (BFR)/BS, BFR/BV, and ObS/BS, in accordance with the standard nomenclature described by Parfitt *et al.* [17]. In the present study, the region of cancellous bone measured was 1–4 mm distal to the lower margin of the growth plate in the proximal tibia, which consists of secondary spongiosa. Cells showing positive staining for TRAP were counted in the region from the distal end of the growth plate to 0.2 mm from the growth plate, and the number of osteoclasts (N.Oc) and osteoclast surface (OcS) per BS were calculated. The measured parameters for cortical bone were total tissue area (Tt Ar), marrow area (Ma Ar), endocortical ES, periosteal and endocortical BS, sLS, dLS, and interlabel width. These data were used to calculate cortical bone area (Ct Ar), endocortical ES/BS, and periosteal and endocortical MS/BS [(sLS/2+dLS)/BS], MAR, and BFR/BS.

Statistical analysis

All the data was expressed as means and standard deviation (SD). Multiple comparisons of data among the groups were performed by analysis of variance (ANOVA) with Fisher's protected least significant difference (PLSD) test. All statistical analyses were performed using the Stat View J-5.0 program on a Macintosh computer. A significance level of $P<0.05$ was used for all the comparisons.

Results

Body weight and biochemical markers (Table 1 and Fig. 1)

The initial body weight did not differ significantly among the four groups. OVX was associated with an increase in the body weight of the animals. Neither alendronate nor alfacalcidol affected the body weight of the ovariectomized animals.

OVX increased the serum OC and urinary DPD levels, and decreased the serum calcium levels. Alendronate prevented the elevation of the urinary DPD level. On the other hand, alfacalcidol enhanced the elevation of both the markers and also increased the serum phosphorus level.

Bone histomorphometic analysis of the cancellous bone of the proximal tibial metaphysis (Fig. 2 and Table 2)

OVX decreased cancellous BV/TV and Tb N and

Table 1. Body weight and serum calcium and phosphorus

	Initial body weight (g)	Final body weight (g)	Calcium (mg/dl)	Phosphorus (mg/dl)
Sham	364 ± 33	341 ± 22	10.5 ± 0.7	5.5 ± 0.9
OVX				
Vehicle	364 ± 29	404 ± 26[a]	9.6 ± 0.5[a]	5.7 ± 0.5
Alendronate	363 ± 35	380 ± 26[a]	9.4 ± 0.3[a]	5.2 ± 0.3
Alfacalcidol	369 ± 29	378 ± 23[a]	10.0 ± 0.2[ac]	7.0 ± 0.5[abc]

Data are expressed as mean ± SD. ANOVA with Fisher's PLSD test was used to compare the data among the groups. [a]: significant vs Sham, [b]: significant vs Vehicle, [c]: significant vs Alendronate.

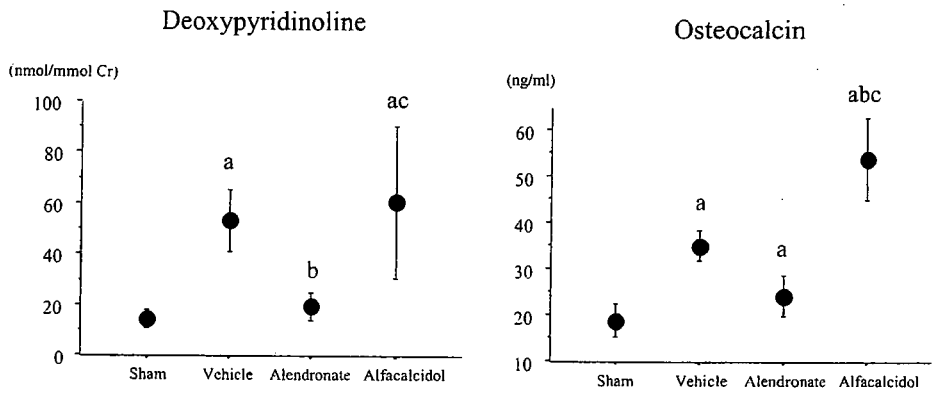

Fig 1. Bone markers Data are expressed as mean ± SD. ANOVA with Fisher's PLSD test was used to compare the data among the groups. a: significant vs Sham, b: significant vs Vehicle, c: significant vs Alendronate.

increased Tb Sp, as a result of increased bone resorption (N.Oc/BS, OcS/BS) and bone formation (ObS/BS, MS/BS, MAR, BFR/BS, BFR/BV). Alendronate prevented these changes of the structural parameters, primarily by suppressing bone resorption (ES/BS, N.Oc/BS, OcS/BS) and bone formation (ObS/BS, MS/BS, MAR, BFR/BS, BFR/BV). However, suppression of bone formation (MS/BS, BFR/BS, BFR/BV) was marked. Alfacalcidol increased cancellous BV/TV and Tb Th to beyond the values obtained in the sham-operated controls, and prevented the alterations of Tb N and Tb Sp, primarily by mildly suppressing bone resorption (ES/BS, N.Oc/BS, OcS/BS) and bone formation (MS/BS, BFR/BS, BFR/BV). The effect of alfacalcidol on cancellous BV/TV was greater than that of alendronate, because the decreases of MS/BS, BFR/BS, and BFR/BV induced by alfacalcidol were comparatively mild, and ObS/BS and MAR were maintained by alfacalcidol.

Bone histomorphometric analysis of the cortical bone of the tibial diaphysis (Fig. 3 and Table 3)

OVX did not affect Tt At, Ct Ar, or Ma Ar, despite increased periosteal bone formation (MS/BS, MAR, BFR/BS) and endocortical bone resorption (ES/BS). Alendronate did not affect Tt At, Ct Ar or Ma Ar, despite suppressed endocortical bone resorption (ES/BS). Alfacalcidol increased Tt At and Ct Ar as compared with the values in the OVX controls, as a result of increased periosteal and endocortical bone formation (MS/BS, MAR, BFR/BS).

Biomechanical test of the femur (Fig. 4)

OVX decreased the maximum load and stiffness of the femoral distal metaphysis, without any effect on the mechanical properties of the femoral diaphysis. Alendronate did not affect any of the mechanical properties of the femoral distal metaphysis or diaphysis,

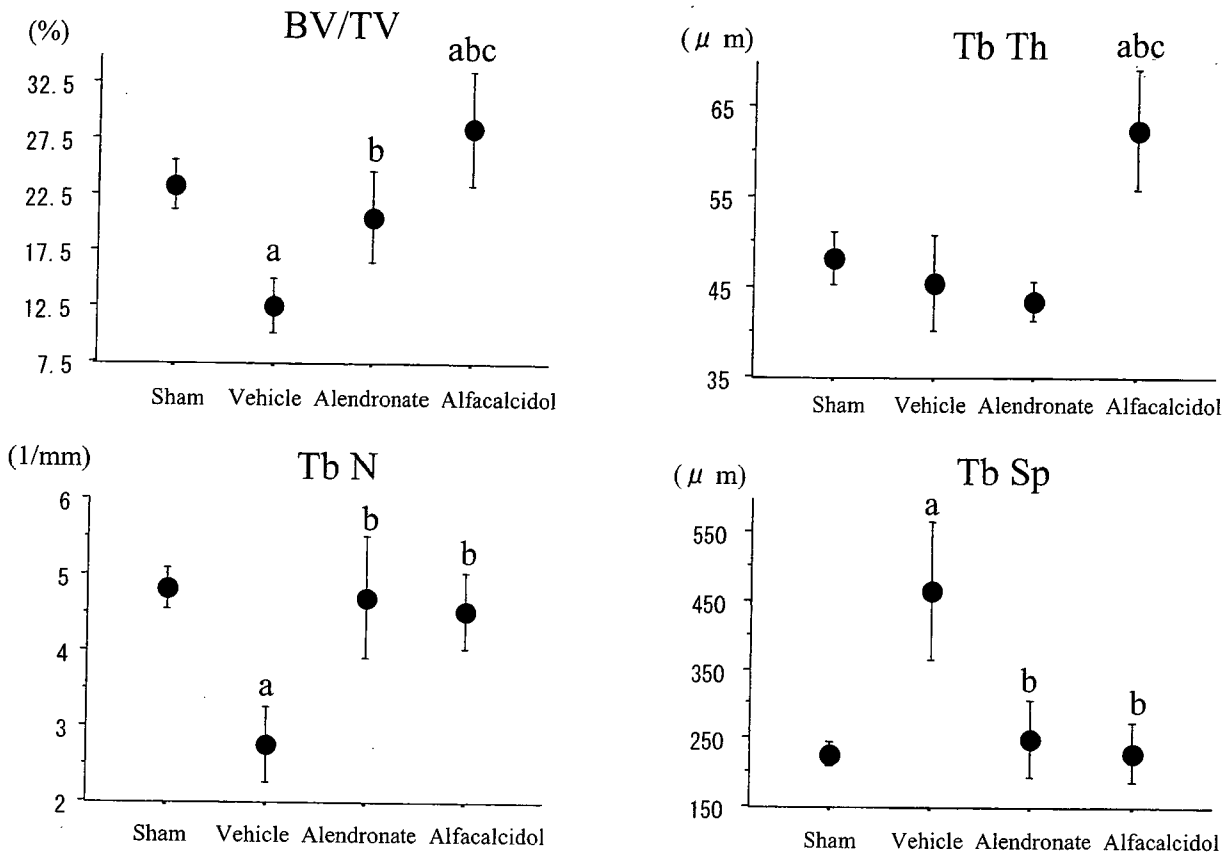

Fig 2. Bone histomorphometric analysis of the cancellous bone of the proximal tibial metaphysis. –Structural parameters– Data are expressed as mean ± SD. ANOVA with Fisher's PLSD test was used to compare the data among the groups. a: significant vs Sham, b: significant vs Vehicle, c: significant vs Alendronate. BV/TV: bone volume/total tissue volume, Tb N: trabecular number, Tb Th: trabecular thickness, Tb Sp: trabecular separation.

Table 2. Histomorphometric analysis of the cancellous bone of the proximal tibial metaphysis –Formative and resorptive variables–

	ES/BS (%)	N.Oc/BS (#/mm)	OcS/BS (%)	ObS/BS (%)	MS/BS (%)	MAR (μm/day)	BFR/BS (μm³/μm²/day)	BFR/BV (%/year)
Sham	11.6 ± 3.7	1.75 ± 0.10	5.4 ± 0.7	10.4 ± 2.4	13.3 ± 2.0	0.44 ± 0.05	5.8 ± 0.8	74 ± 12
OVX								
Vehicle	11.5 ± 2.8	4.12 ± 1.05[a]	14.1 ± 3.0[a]	17.7 ± 3.7[a]	29.5 ± 4.0[a]	0.75 ± 0.14[a]	22.3 ± 6.3[a]	297 ± 68[a]
Alendronate	5.8 ± 1.6[ab]	1.66 ± 0.29[b]	5.3 ± 1.0[b]	14.1 ± 2.1[ab]	8.3 ± 2.3[ab]	0.44 ± 0.10[b]	3.7 ± 1.4[b]	52 ± 22[b]
Alfacalcidol	8.4 ± 1.6[abc]	1.99 ± 0.35[b]	7.1 ± 1.3[bc]	18.8 ± 2.8[ac]	22.0 ± 4.2[abc]	0.70 ± 0.06[ac]	15.5 ± 3.4[abc]	152 ± 35[abc]

Data are expressed as mean ± SD. ANOVA with Fisher's PLSD test was used to compare the data among the groups. [a]: significant vs Sham, [b]: significant vs Vehicle, [c]: significant vs Alendronate. ES: eroded surface, BS: bone surface, N.O c: number of osteoclast, ObS: osteoblast surface, MS: mineralizing surface, MAR: mineral apposition rate, BFR: bone formation rate, BV: bone volume.

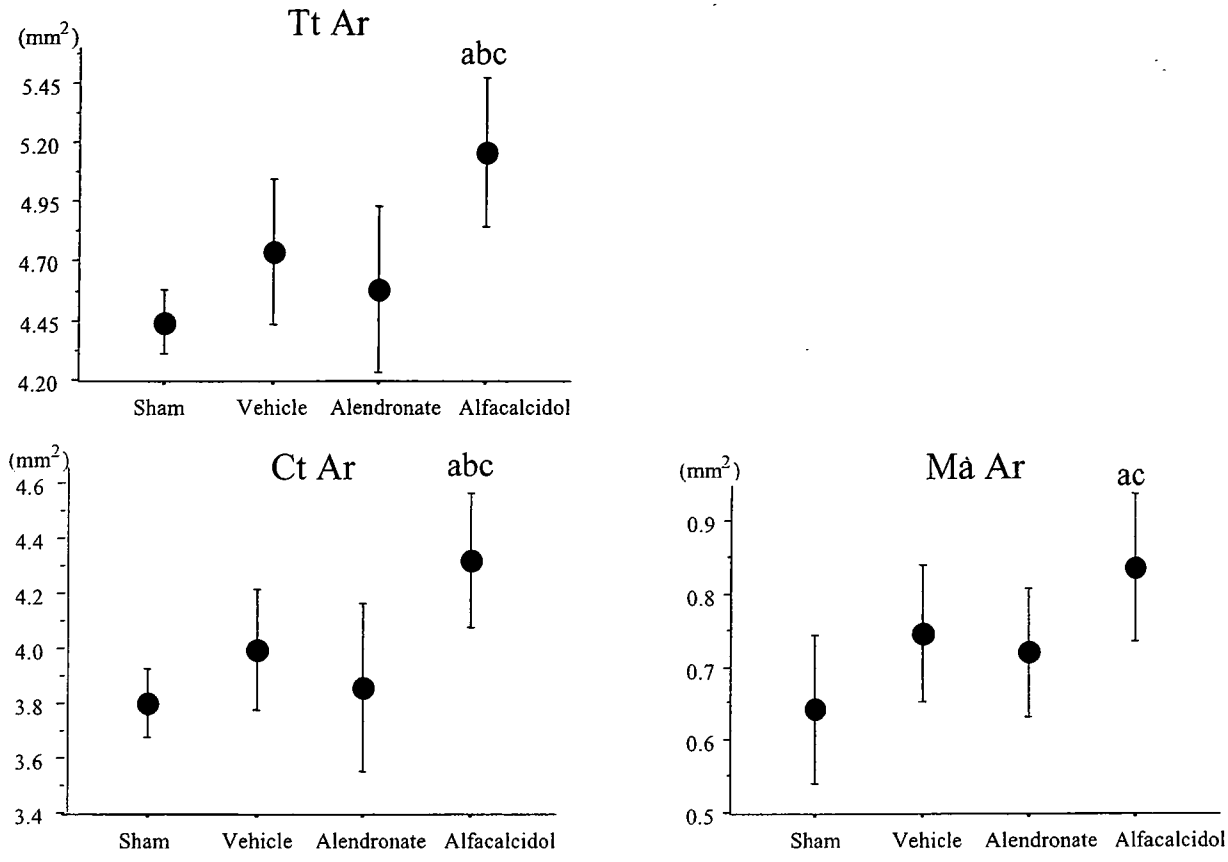

Fig 3. Bone histomorphometric analysis of the cortical bone of the tibial diaphysis. –Structural parameters– Data are expressed as mean ± SD. ANOVA with Fisher's PLSD test was used to compare the data among the groups. a: significant vs Sham, b: significant vs Vehicle, c: significant vs Alendronate. Tt Ar: Total tissue area, Ct Ar: cortical area, Ma Ar: marrow area.

Table 3. Histomorphometric analysis of the cortical bone of the tibial diaphysis –Formative and resorptive variables–

	Periosteal			Endocortical			
	MS/BS (%)	MAR (μm/day)	BFR/BS (μm³/μm²/day)	ES/BS (%)	MS/BS (%)	MAR (μm/day)	BFR/BS (μm³/μm²/day)
Sham	4.9 ± 4.5	0.86 ± 0.11	4.5 ± 5.0	41.0 ± 9.2	4.9 ± 0.8	0.16 ± 0.22	0.82 ± 1.2
OVX							
Vehicle	61.6 ± 19.0[a]	1.18 ± 0.20[a]	73.0 ± 24.0[a]	62.3 ± 9.4[a]	11.4 ± 5.2[a]	0.53 ± 0.17	5.65 ± 2.00
Alendronate	59.9 ± 15.5[a]	1.11 ± 0.25[a]	67.7 ± 23.9[a]	36.7 ± 11.3[b]	10.3 ± 0.5	0.28 ± 0.36	2.72 ± 3.81
Alfacalcidol	80.2 ± 11.5[abc]	1.58 ± 0.19[abc]	127.5 ± 25.9[abc]	38.4 ± 11.3[b]	26.1 ± 12.6[abc]	1.34 ± 0.29[abc]	35.80 ± 19.18[abc]

Data are expressed as mean ± SD. ANOVA with Fisher's PLSD test was used to compare the data among the groups. [a]: significant vs Sham, [b]: significant vs Vehicle, [c]: significant vs Alendronate. MS: mineralizing surface, BS: bone surface, MAR: mineral apposition rate, BFR: bone formation rate, ES: eroded surface.

whereas alfacalcidol increased the maximum load and breaking energy of the femoral distal metaphysis and the maximum load and stiffness of the femoral diaphysis beyond the values obtained in the sham-operated controls.

Discussion

The present study demonstrated that alendronate prevented the decrease in cancellous BV/TV induced by OVX by suppressing bone turnover without any effect

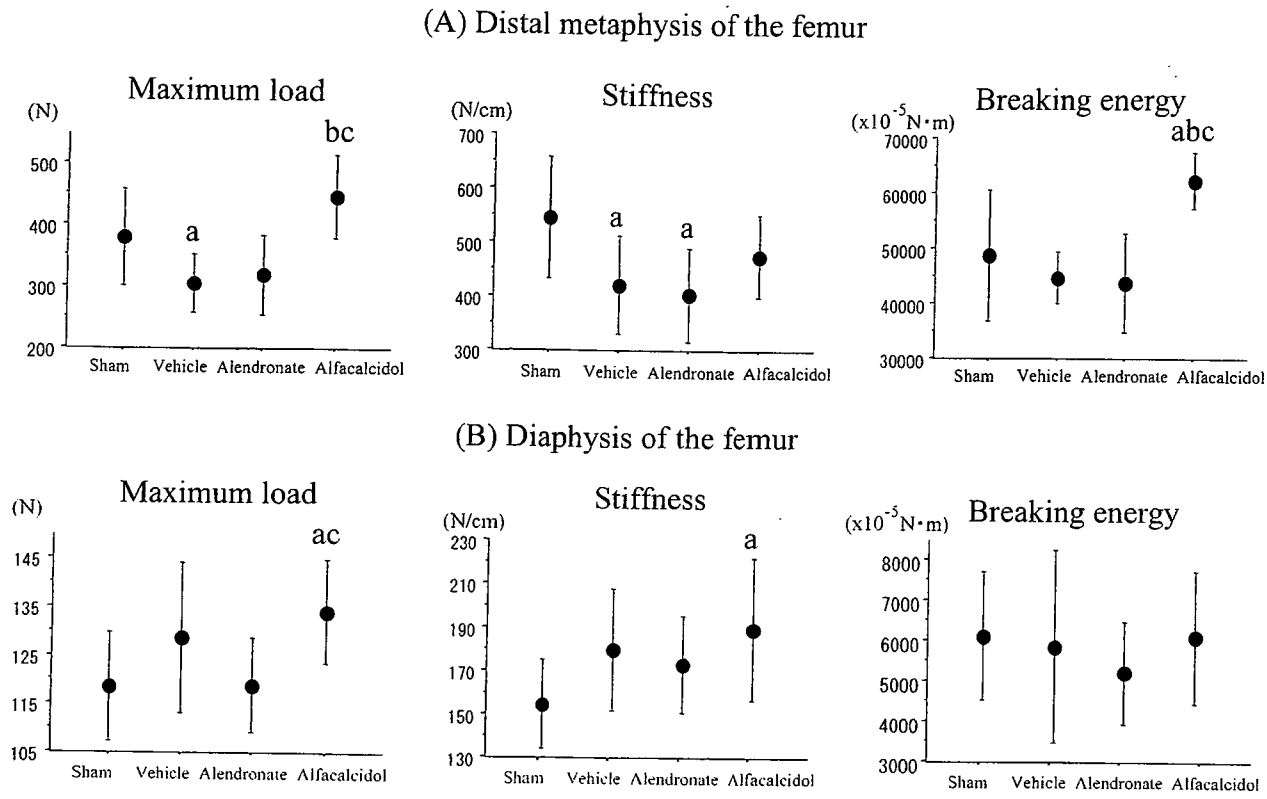

Fig 4. Mechanical properties of the femur Data are expressed as mean ± SD. ANOVA with Fisher's PLSD test was used to compare the data among the groups. a: significant vs Sham, b: significant vs Vehicle, c: significant vs Alendronate.

on Ct Ar. On the other hand, alfacalcidol increased both cancellous BV/TV and Ct Ar by mildly decreasing cancellous bone turnover as indicated by bone histomorphometric analysis and increasing periosteal and endocortical bone formation. The effect of alfacalcidol at the present dose on cancellous BV/TV was greater than that of alendronate, because the decrease of bone turnover by alfacalcidol was comparatively mild, and bone formation was maintained by alfacalcidol. Alfacalcidol, but not alendronate, increased the maximum load of the femoral distal metaphysis and femoral diaphysis. Thus, the present study clearly showed the differential effects of alendronate and alfacalcidol on cancellous and cortical bone mass and bone mechanical properties in ovariectomized rats.

In the present study, OVX increased bone turnover, resulting in the loss of cancellous BV/TV, and Tb N, and the deterioration of the maximum load of the femoral distal metaphysis. However, neither the loss of Tt Ar, and Ct Ar, nor the deterioration of the mechanical properties of the femoral diaphysis was observed following OVX. The bone loss and deterioration of mechanical properties following OVX were observed primarily in regions rich in cancellous bone.

Bisphosphonates inhibit osteoclast-mediated bone resorption. Because of coupling of bone resorption and bone formation, suppression of bone resorption by bisphosphonates is followed by a reduction in bone formation. In other words, bisphosphonates decrease bone turnover. In the present study, the bisphosphonate, alendronate prevented a decrease in cancellous BV/TV in ovariectomized rats by suppressing bone turnover, without exerting any effect on Ct Ar, or maximum load of the femoral distal metaphysis and femoral diaphysis, despite suppressed endocortical bone resorption and maintained periosteal bone formation. Risedronate and pamidronate have been reported to prevent the loss of BMD and the mechanical properties of the femoral distal metaphysis, without having any effect on BMD or the mechanical properties of the femoral diaphysis in sciatic neurectomized and tail-suspended rats, respec-

tively [12, 13]. Furthermore, alendronate and risedronate have also been reported to effectively prevent immobilization (hindlimb-bandage)-induced loss of BMD and the mechanical properties of the femoral metaphysis [15]. These results suggest that bisphosphonates could prevent BMD loss in cancellous bone of hindlimb-immobilized or tail-suspended rats, but not the loss of BMD and the mechanical properties of cortical bone. Clinically, alendronate has been shown to markedly increase BMD of the lumbar spine which is rich in cancellous bone and reduce the incidence of vertebral fractures, but it does not affect metacarpal cortical BMD in postmenopausal women with osteoprosis [11, 14, 23]. All of these results demonstrate that alendronate is effective against the loss of bone mass and bone mechanical properties at skeletal sites rich in cancellous bone.

Despite inducing improvement of cancellous BV/TV, alendronate had no effect on the mechanical properties of the femoral distal metaphysis. Very few studies have clearly shown the beneficial effect of preventive treatment with alendronate alone on the mechanical properties of skeletal sites rich in cancellous bone in ovariectomized rats. Sato *et al.* [19] reported that long-term treatment with alendronate attenuated cancellous BV/TV loss, but scarcely affected the mechanical properties of the lumbar vertebrae in ovariectomized rats, because of marked suppression of bone formation. This result suggests that marked suppression of bone formation can also affect bone quality in ovariectomized rats. In the present study, marked suppression of bone formation might explain the non-significant effect of alendroante on the mechanical properties of the femoral distal metaphysis. It has been established that alendronate (10 mg/day) markedly increases lumbar and femoral neck BMD and reduces the incidence of vertebral and nonvertebral fractures in postmenopausal women with osteoporosis [2, 3, 5]. Thus, no significant effect of alendronate on the mechanical properties of the femoral distal metaphysis in the present study might possibly be attributable to the deterioration of bone quality caused by its high-dose administration.

The active vitamin D, 1α-hydroxyvitamin D_3 (alfacalcidol), is the prodrug of 1α, 25-dihydroxyvitamin D_3, which stimulates calcium absorption in the intestine, enhances calcium reabsorption in the kidney, suppresses parathyroid hormone secretion, and regulates bone formation as well as bone resorption [4, 18]. An experimental study clearly showed that alfacalcidol caused a dose-dependent suppression of bone resorption and yet maintained or even stimulated bone formation, as reflected by the increases in the serum OC levels and BFR/BS at both cancellous and cortical bone sites, resulting in an increase in BMD and improvement of mechanical properties in ovariectomized rats [21]. In the present study, alfacalcidol increased cancellous BV/TV, Tb Th, and Ct Ar in ovariectomized rats by mildly decreasing bone resorption, but maintaining bone formation, increasing periosteal and endocortical bone formation, and preventing an increase of endocortical bone resorption. Alfacalcidol also increased the maximum load of the femoral distal metaphysis and femoral diaphysis. These results were consistent with those of a previous study [21]. Clinically, alfacalcidol maintains BMD of the metacarpus, which consists of cortical bone, and the lumbar spine, which is rich in cancellous bone, and decreases the incidence of vertebral fractures in patients with postmenopausal osteoporosis [8, 16]. All of these results suggest that alfacalcidol may mildly affect both cancellous and cortical bone mass and bone mechanical properties. However, alfacalcidol increased bone turnover, as evaluated by urinary DPD and serum OC levels, which reflect both cancellous and cortical bone turnover.

Clinically, randomized controlled head-to-head trials have demonstrated that alendronate (5 mg/day) is more effective than alfacalcidol (1 μg/day) in increasing lumbar BMD and reducing the incidence of vertebral fractures in Japanese postmenopausal women with osteoporosis [14, 23]. Nevertheless, in the present study, the effect of alfacalcidol (0.5 μg/kg) on cancellous BV/TV was greater than that of alendronate (2.5 mg/kg), and only alfacalcidol increased the maximum load of the femoral distal metaphysis, presumably because the decrease of bone turnover by alfacalcidol administration was comparatively mild as compared with that following alendronate administration, and bone formation was maintained by alfacalcidol. This discrepancy may be due to a differential response of cancellous bone to alfacalcidol between ovariectomized rats and postmenopausal women (human); the beneficial effects of alfacalcidol might be greater on rat bones than on human bones. Only alfacalcidol increased Ct Ar and

the maximum load of the femoral diaphysis. Thus, it would be of interest to investigate the comparative effect of alendronate and alfacalcidol on the incidence of nonvertebral fractures by further clinical trials.

In conclusion, the strengths of the present study included the detailed bone histomorphometric analyses of cancellous and cortical bone, the measurement of biochemical markers, and the measurement of the bone mechanical properties. The results showed that alendronate prevented the decrease in cancellous bone mass observed in ovariectomized rats, without exerting any effect on the cortical bone mass. On the other hand, alfacalcidol increased both cancellous and cortical bone mass. Alfacalcidol, but not alendronate, increased the maximum load of the bone at both sites rich in cortical and cancellous bone. Thus, the present study clearly showed the differential effects of alendronate and alfacalcidol on cancellous and cortical bone mass and bone mechanical properties in ovariectomized rats.

References

1. Azuma, Y., Oue, Y., Kanatani, H., Ohta, T., Kiyoki, M., and Komoriya, K. 1998. Effects of continuous alendronate treatment on bone mass and mechanical properties in ovariectomized rats: comparison with pamidronate and etidronate in growing rats. *J. Pharmacol. Exp. Ther.* 286: 128–135.
2. Black, D.M., Cummings, S.R., Karpf, D.B., Cauley, J.A., Thompson, D.E., Nevitt, M.C., Bauer, D.C., Genant, H.K., Haskell, W.L., Marcus, R., Ott, S.M., Torner, J.C., Quandt, S.A., Reiss, T.F., and Ensrud, K.E. 1996. Fracture Intervention Trial Research Group. Randomised trial of effect of alendronate on risk of fracture in women with existing vertebral fractures. *Lancet* 348: 1535–1541.
3. Bone, H.G., Hosking, D., Devogelaer, J.P., Tucci, J.R., Emkey, R.D., Tonino, R.P., Rodriguez-Portales, J.A., Downs, R.W., Gupta, J., Santora, A.C., and Liberman, U.A. Alendronate Phase III Osteoporosis Treatment Study Group (2004) Ten years' experience with alendronate for osteoporosis in postmenopausal women. *N. Engl. J. Med.* 350: 1189–1199.
4. Brommage, R. and DeLuca, H.F. 1985. Evidence that 1,25-dihydroxyvitamin D_3 is the physiologically active metabolite of vitamin D_3. *Endocr. Rev.* 6: 491–511.
5. Cummings, S.R., Black, D.M., Thompson, D.E., Applegate, W.B., Barrett-Connor, E., Musliner, T.A., Palermo, L., Prineas, R., Rubin, S.M., Scott, J.C., Vogt, T., Wallace, R., Yates, A.J., and LaCroix, A.Z. 1998. Effect of alendronate on risk of fracture in women with low bone density but without vertebral fractures: results from the Fracture Intervention Trial. *J.A.M.A.* 280: 2077–2082.
6. da Paz, L.H., de Falco, V., Teng, N.C., dos Reis, L.M., Pereira, R.M., and Jorgetti, V. 2001. Effect of 17beta-estradiol or alendronate on the bone densitometry, bone histomorphometry and bone metabolism of ovariectomized rats. *Braz. J. Med. Biol. Res.*34: 1015–1022.
7. Erben, R.G. 1997. Embedding of bone samples in methylmethacrylate: an improved method suitable for bone histomorphometry, histochemistry, and immunohistochemistry. *J. Histochem. Cytochem.* 45: 307–313.
8. Fujita, T. 1990 Studies on osteoporosis in Japan. *Metabolism* 39 (Suppl 1): 39–42.
9. Giavaresi, G., Fini, M., Gnudi, S., Aldini, N.N., Rocca, M., Carpi, A., and Giardino, R. 2001. Comparison of calcitonin, alendronate and fluorophosphate effects on ovariectomized rat bone. *Biomed. Pharmacother.* 55: 397–403.
10. Ito, M., Nishida, A., Koga, A., Ikeda, S., Shiraishi, A., Uetani, M., Hayashi, K., and Nakamura, T. 2002. Contribution of trabecular and cortical components to the mechanical properties of bone and their regulating parameters. *Bone* 31: 351–358.
11. Iwamoto, J., Takeda, T., Sato, Y., and Uzawa, M. 2004. Effects of alendronate on metacarpal and lumbar bone mineral density, bone resorption, and chronic back pain in postmenopausal women with osteoporosis. *Clin. Rheumatol.* 23: 383–389.
12. Iwamoto, J., Seki, A., Takeda, T., Sato, Y., and Yamada, H. 2005. Effects of Risedronate on Femoral Bone Mineral Density and Bone Strength in Sciatic Neurectomized Young *Rats. J. Bone Miner. Metab.* 23: 456–462.
13. Kodama, Y., Nakayama, K., Fuse, H., Fukumoto, S., Kawahara, H., Takahashi, H., Kurokawa, T., Sekiguchi, C., Nakamura, T., and Matsumoto, T. 1997. Inhibition of bone resorption by pamidronate cannot restore normal gain in cortical bone mass and strength in tail-suspended rapidly growing rats. *J. Bone Miner. Res.* 12: 1058–1067.
14. Kushida, K., Shiraki, M., Nakamura, T., Kishimoto, H., Morii, H., Yamamoto, K., Kaneda, K., Fukunaga, M., Inoue, T., Nakashima, M., and Orimo, H. 2004. Alendronate reduced vertebral fracture risk in postmenopausal Japanese women with osteoporosis: a 3-year follow-up study. *J. Bone Miner. Metab.* 22: 462–468.
15. Mosekilde, L., Thomsen, J.S., Mackey, M.S., and Phipps, R.J. 2000. Treatment with risedronate or alendronate prevents hind-limb immobilization-induced loss of bone density and strength in adult female rats. *Bone* 27: 639–645.
16. Orimo, H., Shiraki, M., Hayashi, Y., Hoshino, T., Onaya, T., Miyazaki, S., Kurosawa, H., Nakamura, T., and Ogawa, N. 1994. Effects of 1 alpha-hydroxyvitamin D_3 on lumbar bone mineral density and vertebral fractures in patients with postmenopausal osteoporosis. *Calcif. Tissue Int.* 54: 370–376.
17. Parfitt, A.M., Drezner, M.K., Glorieux, FH., Kanis, J.A., Malluche, H., Meunier, P.J., Ott, S.M., and Recker, R.R. 1987. Bone histomorphometry: standardization of nomenclature, symbols, and units. Report of the ASMBR

Histomorphometry Nomenclature Committee. *J. Bone Miner. Res.* 2: 595–610.

18. Reichel, H., Koeffler, H.P., and Norman, A.W. 1989. The role of the vitamin D endocrine system in health and disease. *N. Engl. J. Med.* 320: 980–991.
19. Sato, M., Bryant, H.U., Iversen, P., Helterbrand, J., Smietana, F., Bemis, K., Higgs, R., Turner, C.H., Owan, I., Takano, Y., and Burr, D.B. 1996. Advantages of raloxifene over alendronate or estrogen on nonreproductive and reproductive tissues in the long-term dosing of ovariectomized rats. *J. Pharmacol. Exp. Ther.* 279: 298–305.
20. Seedor, J.G., Quartuccio, H.A., and Thompson, D.D. 1991. The bisphosphonate alendronate (MK-217) inhibits bone loss due to ovariectomy in rats. *J. Bone Miner. Res.* 6: 339–346.
21. Shiraishi, A., Takeda, S., Masaki, T., Higuchi, Y., Uchiyama, Y., Kubodera, N., Sato, K., Ikeda, K., Nakamura, T., Matsumoto, T., and Ogata, E. 2000. Alfacalcidol inhibits bone resorption and stimulate formation in an ovariectomized rat model of osteoporosis: distinct actions from estrogen. *J. Bone Miner. Res.* 15: 770–779.
22. Shiraishi, A., Higashi, S., Masaki, T., Saito, M., Ito, M., Ikeda, S., and Nakamura, T. 2002. A comparison of alfacalcidol and menatetrenone for the treatment of bone loss in an ovariectomized rat model of osteoporosis. *Calcif. Tissue Int.* 71: 69–79.
23. Shiraki, M., Kushida, K., Fukunaga, M., Kishimoto, H., Taga, M., Nakamura, T., Kaneda, K., Minaguchi, H., Inoue, T., Morii, H., Tomita, A., Yamamoto, K., Nagata, Y., Nakashima, M., and Orimo, H. 1999. The Alendronate Phase III Osteoporosis Treatment Research Group. A double-masked multicenter comparative study between alendronate and alfacalcidol in Japanese patients with osteoporosis. *Osteoporos. Int.* 10: 183–192.

pH-Responsive Three-Layered PEGylated Polyplex Micelle Based on a Lactosylated ABC Triblock Copolymer as a Targetable and Endosome-Disruptive Nonviral Gene Vector

Motoi Oishi,[†] Kazunori Kataoka,*[,‡,#] and Yukio Nagasaki*[,†]

Tsukuba Research Center for Interdisciplinary Materials Science (TIMS), University of Tsukuba, 1-1-1 Ten-noudai, Tsukuba, Ibaraki 305-8573, Japan, Department of Materials Engineering, Graduate School of Engineering, The University of Tokyo, 7-3-1 Hongo, Bunkyo-ku, Tokyo 113-8656, Japan, and Division of Clinical Biotechnology, Center for Disease Biology and Integrative Medicine, Graduate School of Medicine, The University of Tokyo, 7-3-1 Hongo, Bunkyo-ku, Tokyo 113-0033, Japan. Received December 24, 2005; Revised Manuscript Received February 21, 2006

Nonviral vectors for gene therapy have recently received an increased impetus because of the inherent safety problems of the viral vectors, while their transfection efficiency is generally low compared to the viral vectors. The lack of the ability to escape from the endosomal compartments is believed to be one of the critical barriers to the intracellular delivery of noviral gene vectors. This study was devoted to the design and preparation of a novel ABC triblock copolymer for constructing a pH-responsive and targetable nonviral gene vector. The copolymer, lactosylated poly(ethylene glycol)-*block*-poly(silamine)-*block*-poly[2-(*N,N*-dimethylamino)ethyl methacrylate] (Lac-PEG-PSAO-PAMA), consists of lactosylated poly(ethylene glycol) (A-segment), a pH-responsive polyamine segment (B-segment), and a DNA-condensing polyamine segment (C-segment). The Lac-PEG-PSAO-PAMA spontaneously associated with plasmid DNA (pDNA) to form three-layered polyplex micelles with a PAMA/pDNA polyion complex (PIC) core, an uncomplexed PSAO inner shell, and a lactosylated PEG outer shell, as confirmed by ^{1}H NMR spectroscopy. Under physiological conditions, the Lac-PEG-PSAO-PAMA/pDNA polyplex micelles prepared at an N/P (number of amino groups in the copolymer/number of phosphate groups in pDNA) ratio above 3 were found to be able to condense pDNA, thus adopting a relatively small size (< 150 nm) and an almost neutral surface charge ($\zeta \sim +5$ mV). The micelle underwent a pH-induced size variation (pH = 7.4, 132.6 nm → pH = 4.0, 181.8 nm) presumably due to the conformational changes (globule-rod transition) of the uncomplexed PSAO chain in response to pH, leading to swelling of the free PSAO inner shell at lowered pH while retaining the condensed pDNA in the PAMA/pDNA PIC core. Furthermore, the micelles exhibited a specific cellular uptake into HuH-7 cells (hepatocytes) through asialoglycoprotein (ASGP) receptor-mediated endocytosis and achieved a far more efficient transfection ability of a reporter gene compared to the Lac-PEG-PSAO/pDNA and Lac-PEG-PAMA/pDNA polyplex micelles composed of the diblock copolymers and pDNA. The effect of hydroxychloroquine as an endosomolytic agent on the transfection efficiency was not observed for the Lac-PEG-PSAO-PAMA/pDNA polyplex micelles, whereas the nigericin treatment of the cell as an inhibitor for the endosomal acidification induced a substantial decrease in the transfection efficiency, suggesting that the protonation of the free PSAO inner shell in response to a pH decrease in the endosome might lead to the disruption of the endosome through buffering of the endosomal cavity. Therefore, the polyplex micelle composed of ABC (ligand-PEG/pH-responsive segment/DNA-condensing segment) triblock copolymer would be a promising approach to a targetable and endosome disruptive nonviral gene vector.

INTRODUCTION

Nonviral vectors for gene therapy have recently received increased attention because of the concerns over the safety issues of viral vectors, including immunogenicity, oncogenicity, and potential virus recombination (*1*–*3*). Most of the nonviral vectors developed so far, however, show low transfection efficiency compared to the viral vectors, because the latter have evolved multi-functionality to overcome the critical barrier to efficient gene delivery by directing the specific cellular uptake and enhancing transport to the cytoplasm from the endosomal compartment. Recently, a new class of nonviral gene vectors has been developed based on the supramolecular assembly between plasmid DNA (pDNA) and poly(ethylene glycol) (PEG)-*block*-polyamine copolymers (polyplex micelles) (*4*–*10*). Because of the highly dense PEG shell surrounding the polyion complex (PIC) core, the polyplex micelles exhibited excellent solubility in aqueous media, high tolerability toward nuclease degradation, and minimal interaction with biological components, including proteins and cells, compared to the other conventional polyplex and lipoplex systems. Furthermore, ligand-installed polyplex micelles prepared from lactosylated PEG-*block*-poly[2-(*N,N*-dimethylamino)ethyl methacrylate] copolymer and pDNA showed an increase in the cellular uptake through a receptor-mediated endocytosis process compared to those without lactose (ligand) moieties (*11*). To observe an appreciable effect of the ligand molecules on gene expression, however, the presence of hydroxychloroquine (100 μM) as an endosomolytic agent (*12*, *13*) has so far been required. This indicates that endosomal escape should be the most critical

* To whom correspondence should be addressed. (Y.N.) Phone: +81-29-853-5749. Fax: +81-29-853-5749. E-mail: nagasaki@nagalabo.jp; (K.K.) Phone +81-3-5841-7139. Fax: +81-3-5841-7139. E-mail: kataoka@bmw.t.u-tokyo.ac.jp.

† Tsukuba Research Center for Interdisciplinary Materials Science (TIMS), University of Tsukuba.

‡ Department of Materials Engineering, The University of Tokyo.

Division of Clinical Biotechnology, The University of Tokyo.

10.1021/bc050364m CCC: $33.50
Published on Web 04/15/2006

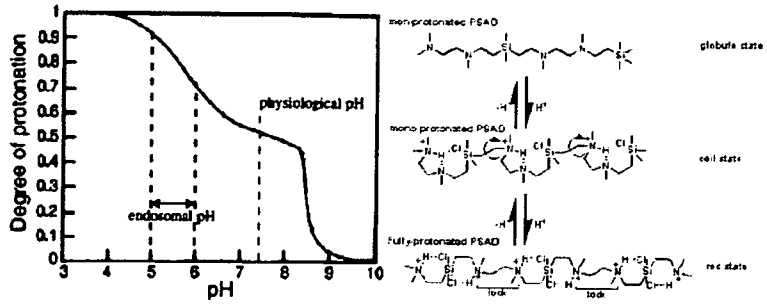

Figure 1. Change in the protonation degree of poly(silamine) (PSAO) with pH accompanying the conformation transition (globule-coil-rod).

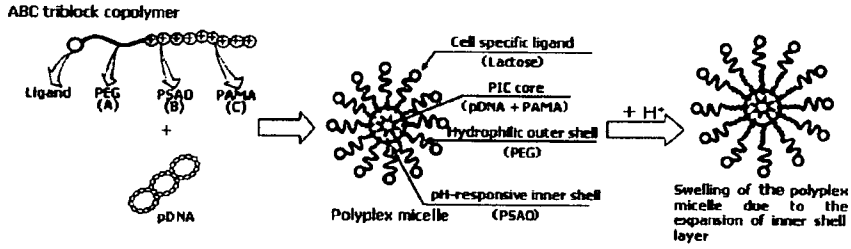

Figure 2. Schematic illustration of the formation of the three-layered polyplex micelle composed of the ABC triblock copolymer and pDNA.

barrier to intracellular gene delivery by polyplex micelles (*14*–*16*). Therefore, approaches are needed to devise polyplex micelles with a function to escape from the endosome where the pH is 1.4−2.4 units lower than the physiological pH of 7.4 (*17*–*20*). In this regard, poly(ethylenimine) (PEI) derivatives are of interest as a pH-responsive polyamine component to accomplish endosomal escape by taking advantage of their substantially lowered value of apparent pK_a (~5.5) ("buffer or proton-sponge effect") (*21*). However, the buffer effect of the PEI segment occurs only when an excess of amino groups with respect to DNA phosphate groups (high N/P ratio) is present in the system, where a considerable amount of the amino groups in PEI is in the free-base form. This fact strongly suggests that free PEI, which is not complexed with pDNA, is likely to play a crucial role in the buffer effect, because amino groups in the PEI/pDNA polyplex generally undergo facilitated protonation due to the zipper effect or the neighboring group effect during the polyion complexation (over-protonation) to decrease the buffering capacity (*22*). Therefore, a strategy is needed to satisfy the prevention of overprotonation of the pH-responsive polyamine segment in the polyplex, as well as the achievement of efficient condensation of pDNA into the PIC core to exert efficient stability. Worth noting in this regard is a concomitant incorporation of the polyamine segment with a high pK_a and one with a low pK_a into a single PEG-based strand, as an ABC triblock copolymer (*23*). A polyamine segment with a high pK_a as the C block preferentially forms a polyion complex with phosphate groups in pDNA (DNA-condensation segment), whereas the pH-responsive polyamine segment (B block) with a comparatively low pK_a, located between the PEG segment (A block) and the pDNA-condensation segment (C block), is expected to retain a substantial fraction of unprotonated amino groups (free-base) even in the polyplex due to the low protonation ability. As a consequence, the polyion complexation between such an ABC triblock copolymer and pDNA may lead to the formation of a three-layered polyplex micelle possessing an unprotonated pH-responsive polyamine segment as an intermediate layer to function as a buffering moiety for facilitated endosomal escape.

We herein synthesized a novel ABC triblock copolymer composed of a targetable and biocompatible polymer segment, a pH-responsive polyamine segment, and a DNA-condensing polyamine segment to form a three-layered polyplex micelle: lactosylated PEG-*block*-poly(silamine) (PSAO) -*block*-poly[2-(*N*,*N*-dimethylamino)ethyl methacrylate] (PAMA) [Lac-PEG-PSAO-PAMA]. Here, PSAO was selected as the pH-responsive polyamine segment showing two-step protonation (Figure 1, $pK_{a1} = 8.6$ and $pK_{a2} = 5.8$) along with a unique conformational transition at the critical pH (*24*–*29*). The unprotonated PSAO is insoluble in water, assuming a globular conformation with high flexibility, whereas fully protonated PSAO is soluble in water, assuming a rodlike conformation with rigid and expanded polymer strands. Such a unique conformational transition (rod-globule transition) can be explained by the rotational hindrance around the polymer chain due to the protonation of the amino groups along with the counteranion binding to the Si atoms (Figure 1). On the other hand, PAMA ($pK_a = 7.2$) is known to condense pDNA to form a compact structure, the size of which is less than 200 nm under physiological conditions (*8*, *30*, *31*). This fact suggests that polyion complexation between the Lac-PEG-PSAO-PAMA and pDNA may form a targetable and endosome disruptive polyplex micelle with a well-defined three-layered structure (Figure 2).

EXPERIMENTAL SECTION

Materials. 2,2′-Azobisisobutyronitrile (AIBN), dicyclohexylcarbodiimide (DCC), *N*-hydroxysuccinimide (NHS), and nigericin (NR) were purchased from Wako and used without further purification. Asialofetuine (ASF) and hydroxychloroquine sulfate (HCQ) were purchased from Sigma and Acros Organics, respectively. Potassium naphthalene was used as a THF solution, whose concentration was determined by titration. Water was purified using a Milli-Q instrument (Millipore). 2-Propanol and diethyl ether (Et_2O) were used as received without further purification. Lysotraker Red DND-99 was purchased from Molecular Probes. Plasmid DNA (pDNA) encoding firefly luciferase (pGL3-Luc, Promega; 5256 bpa) was amplified using EndoFree Plasmid Maxi or Mega kits (QIAGEN). The DNA concentration was determined by reading the absorbance at 260 nm.

Polymer Analysis. ^1H NMR (400 MHz) spectra were obtained in $CDCl_3$, DMSO-d_6, or D_2O (pD = 7.4 and 4.0) with 0.15 M NaCl using a JEOL EX400 spectrometer. Chemical shifts were reported in ppm relative to $CDCl_3$ (δ7.26, ^1H), DMSO-d_6 (δ 2.50, ^1H), or D_2O buffer (δ 4.76, ^1H). Size exclusion chromatography (SEC) was performed using a TOSO

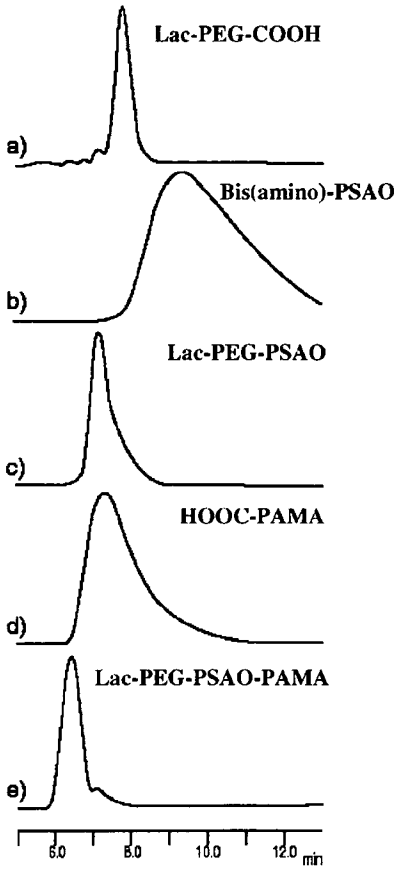

Figure 3. SEC chromatograms of the (a) Lac-PEG-COOH, (b) bis-(amino)-PSAO, (c) Lac-PEG-PSAO block copolymer, (d) HOOC-PAMA, and (e) Lac-PEG-PSAO-PAMA triblock copolymer.

HLC-8020 equipped with an internal refractive index (RI) detector (RID-6A) with the combination of TSK G4000$_{HR}$ and G3000$_{HR}$ columns using THF as the eluent.

Synthesis of Lactose-PEG-*block*-PSAO. Bis(amino)-PSAO was synthesized according to our previous report (*24*−*29*). The Lac-PEG-COOH (0.100 g, 16 μmol) and an excess amount of bis(amino)-PSAO (1.244 g 800 μmol, M_n = 1550, DP = 6) were dissolved in $CHCl_3$ (5.0 mL) together with DCC (6.3 mg, 32 μmol) and NHS (2.3 mg, 20 μmol). The reaction mixture was stirred at room temperature for 72 h. To remove the unreacted bis(amino)-PSAO and other chemicals, the reaction mixture was poured into Et_2O (200 mL). The obtained polymer was further purified by reprecipitation into Et_2O (200 mL) and then freeze-dried with benzene to obtain the lactose-PEG-*b*-PSAO (0.102 g, 83% yield). Figures 3c and 4a, respectively, show the SEC chromatogram and ^{1}H NMR spectrum of Lac-PEG-PSAO with assignment. SEC M_n = 7170, M_w/M_n = 1.15 (calcd. M_n = 7850); ^{1}H NMR ($CDCl_3$, in Figure 4a) δ 0.10 (s, 36H, H_k), 0.63−0.79 (m, 24H, H_j), 1.02 (t, J = 7.3 Hz, 36H, H_i), 1.10 (t, J = 7.1 Hz, 3H, H_i''), 1.16 (t, J = 7.1 Hz, 3H, H_i'), 1.77−2.02 (m, 4H, H_d+H_f), 2.42 (t, J = 7.1 Hz, 2H, H_g), 2.47−2.62 (m, 80H, H_h), 2.62−2.73 (m, 2H, H_c), 3.61 (s, 617H, H_a+H_b+H_e)

Synthesis of Lactose-PEG-*block*-PSAO-*block*-PAMA. A PAMA homopolymer bearing a carboxylic acid group at the α-end (HOOC-PAMA) was synthesized via anionic polymerization of 2-(*N*,*N*-dimethylamino)ethyl methacrylate (*32*) using the allyl alcohol/potassium-naphthalene initiator system, followed by the radical addition of 3-mercaptopropionic acid in the presence of AIBN. The Lac-PEG-PSAO (0.051 g, 7.8 μmol) and an excess amount of HOOC-PAMA bearing a carboxylic acid group at the α-end (0.5017 g, 88.5 μmol, M_n = 5670, DP = 35) were dissolved in $CHCl_3$ (5.0 mL) together with DCC (3.2 mg, 16 μmol) and NHS (1.6 mg, 10 μmol). The reaction mixture was stirred at room temperature for 72 h. To remove the unreacted HOOC-PAMA and other chemicals, the polymer was recovered by precipitation into cold 2-propanol (−15 °C, 200 mL) and centrifuged for 45 min at 6000 rpm. Further purification was carried out by dialyzing against distilled, deionized water (cutoff MW 3500) and then freeze-dried to obtain Lac-PEG-PSAO-PAMA (0.0383 g, 37% yield). Figures 3e and 4b, respectively, show the SEC chromatogram and ^{1}H NMR spectrum of Lac-PEG-PSAO-PAMA with assignment. SEC M_n = 10850, M_w/M_n = 1.29 (calcd. M_n = 13450); ^{1}H NMR ($CDCl_3$, in Figure 4b) δ 0.10 (s, 36H, H_d), 0.63−0.79 (m, 24H, H_c), 0.80−1.16 (m, 94H, H_g), 1.02 (t, J = 7.3 Hz, 42H, H_e), 1.16−2.17 (m, 64H, H_f), 2.23 (s, 185H, H_j), 2.37−2.84 (m, 143H, H_b + H_i), 3.61 (s, 617H, H_a), 4.08 (s, 62H, H_h).

Light Scattering Measurements of Polyplex Micelles. To prepare stock solutions, specific amounts of each of the block copolymers (Lac-PEG-PSAO-PAMA, Lac-PEG-PSAO, and Lac-PEG-PAMA) were dissolved in 10 mM Tris-HCl buffer (pH 7.4) or distilled, deionized water, followed by adjustment of the pH to 7.4. Both solutions were filtered through a 0.1-μm filter to remove dust prior to the measurement. For the dynamic light scattering (DLS) measurements as a function of pH, the Lac-PEG-PSAO-PAMA copolymer in distilled water at pH 7.4 including 0.15 M NaCl was mixed with pDNA at an N/P ratio of 3 [N/P = (amino group in the block copolymer)/(phosphate groups in pDNA)] at pH 7.4 to obtain the final concentration of 33.3 μg/mL of pDNA in the solution. The sample solutions were adjusted to the desired pH using small aliquots of 0.1 or 0.01 M HCl, and the DLS was measured at each pH point (pH = 7.0, 6.5, 6.0, 5.5, 5.0, 4.5, and 4.0).

For the DLS measurements of the samples prepared at various N/P ratios, the block copolymer in 10 mM Tris-HCl buffer (pH 7.4) was mixed with pDNA at various N/P ratios (N/P = 1, 2, 3, 4, 5, 7, and 10), followed by the addition of 10 mM Tris-HCl buffer (pH 7.4) including 0.3 M NaCl to adjust the pDNA concentration (33.3 μg/mL) and the ionic strength of the solution to physiological conditions (0.15 M NaCl).

A light-scattering spectrometer (DLS-7000, Photal, Otsuka Electronics) equipped with a 75 mW Ar-laser that produces a vertically polarized incident beam at λ_0 = 488 nm was used in the present study for the DLS measurements.

During the DLS measurements, the autocorrelation function was analyzed using the cumulant method in which

$$g^{(1)}(\tau) = \exp[-\bar{\Gamma}\tau + (\mu_2/2)\tau^2 - (\mu_3/3!)\tau^3 + \cdots] \quad (1)$$

yielding an average characteristic line width of $\bar{\Gamma}$. The z-averaged diffusion coefficient was obtained from the $\bar{\Gamma}$ based on the following equations:

$$\bar{\Gamma} = Dq^2 \quad (2)$$

$$q = (4\pi n/\lambda)\sin(\theta/2) \quad (3)$$

where q is the magnitude of the scattering vector, n is the refractive index of the solvent, and θ is the detection angle. The hydrodynamic radius, d, can then be calculated using the Stokes−Einstein equation:

$$d = k_B T/(6\pi\eta D) \quad (4)$$

where k_B is the Boltzmann constant, T is the absolute temperature, and η is the viscosity of the solvent. Also, the polydispersity index (PDI = μ_2/Γ^2) was derived from eq 1.

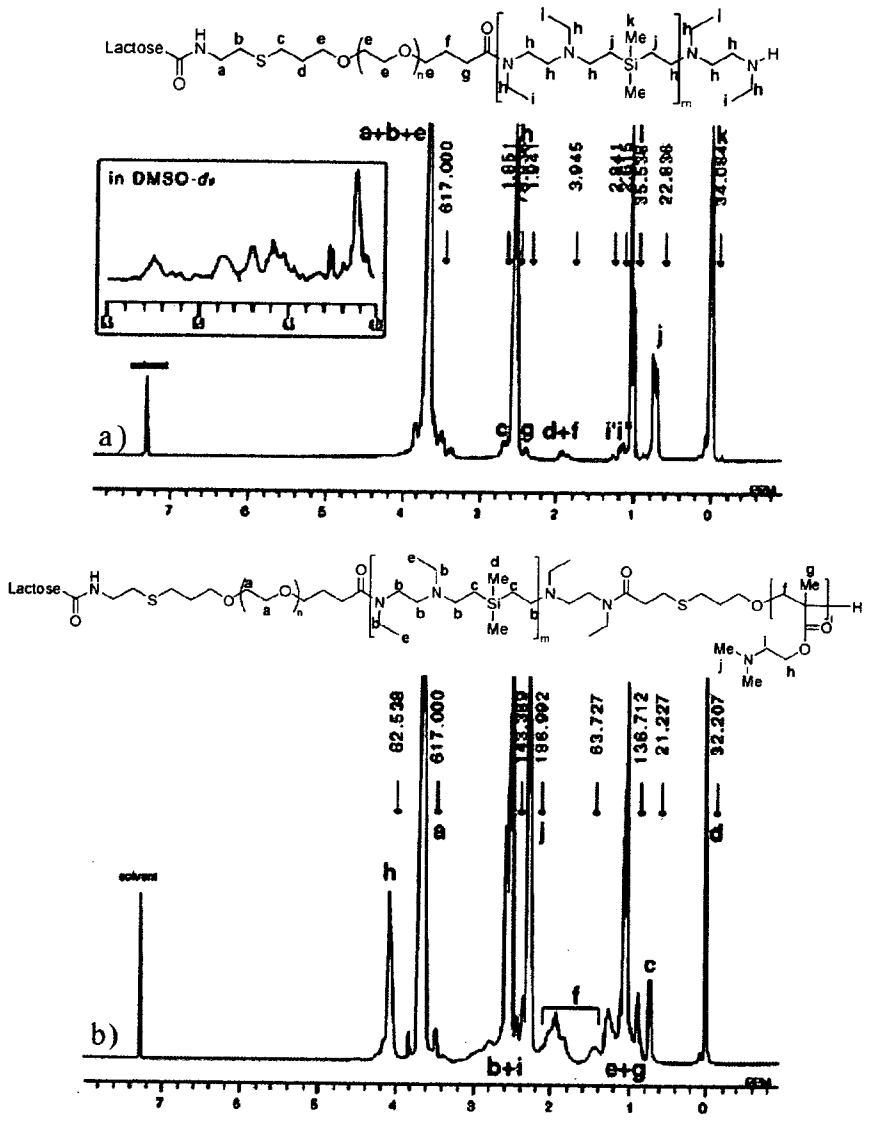

Figure 4. ^{1}H NMR spectra of (a) Lac-PEG-PSAO diblock copolymer and (b) Lac-PEG-PSAO-PAMA triblock copolymer.

Zeta-Potential Measurements. Laser-Doppler electrophoresis measurements of the polyplex micelles were carried out in 10 mM Tris-HCl buffer (pH 7.4) without NaCl (ELS-600, Photal, Otsuka Electronics). From the determined electrophoretic mobility, the zeta-potential (ζ) was calculated according to the Smoluchouski equation as follows:

$$\zeta = 4\pi n\eta\mu u/\epsilon \qquad (5)$$

where η is the viscosity of the solution, u is the electrophoretic mobility, and ϵ is the dielectric constant of the solvent.

Ethidium Bromide Exclusion Assay. The polyplex micelle solutions at various N/P ratios were mixed with ethidium bromide (EtBr) solution, and the final concentration was adjusted to [pDNA] = 20 μg/mL and [EtBr] = 0.4 μg/mL. The fluorescence of the intercalated EtBr was measured on a spectrofluorometer (F-2500, Hitachi) by exciting at 510 nm while monitoring emission at 590 nm.

Agarose Gel Retardation Studies. Aliquots (10 μL) of the above polyplex micelle solutions with various N/P ratios were mixed with 13 μL of running buffer of 3.3 mM Tris-AcOH with 1.0 mM EDTA2Na (pH 7.4) and loaded onto a 0.9 wt % agarose gel (50 V, 2 h). The amount of pDNA was adjusted to 0.3 μg of pDNA/lane. After EtBr (0.5 μg/mL) staining for 1 h, retardation of pDNA was visualized under UV irradiation.

Cell Culture. HuH-7 human cancer cells, derived from a hepatocarcinoma cell line, were obtained from the Cell Resource Center for Biomedical Research, Institute of Development, Aging and Cancer, Tohoku University. The cells were grown in Dulbecco's modified Eagle's medium (DMEM) supplemented with 10% FBS, 100 units/mL penicillin, and 100 μg/mL streptomycin at 37 °C in a humidified 5% CO_2 atmosphere.

Fluorescent Microscopy. Fluorescein isothiocyanate (FITC)-labeled pDNA was prepared using a Label IT nucleic acid labeling kit (Panvera). HuH-7 cells were seeded at a density of 5×10^5 cells/dish in a 35-mm glass bottom dish (Iwaki, Japan) and kept overnight at 37 °C in 5% CO_2 atmosphere. The Lac-PEG-PSAO-PAMA/pDNA polyplex micelles (N/P = 3) were added at a pDNA concentration of 30 μg/mL and incubated at 37 °C in 5% CO_2 atmosphere in the presence or absence of ASF (10 mg/mL) for 60 min. The cells were washed with phosphate buffered saline (PBS) three times and imaged directly in the cell culture medium using an Olympus IX70 with an appropriate filter.

Confocal Fluorescent Microscopy. HuH-7 cells were seeded at a density of 5×10^5 cells/dish in a 35-mm glass bottom dish

Scheme 1. Synthetic Route of Lac-PEG-PSAO-PAMA Block Copolymer

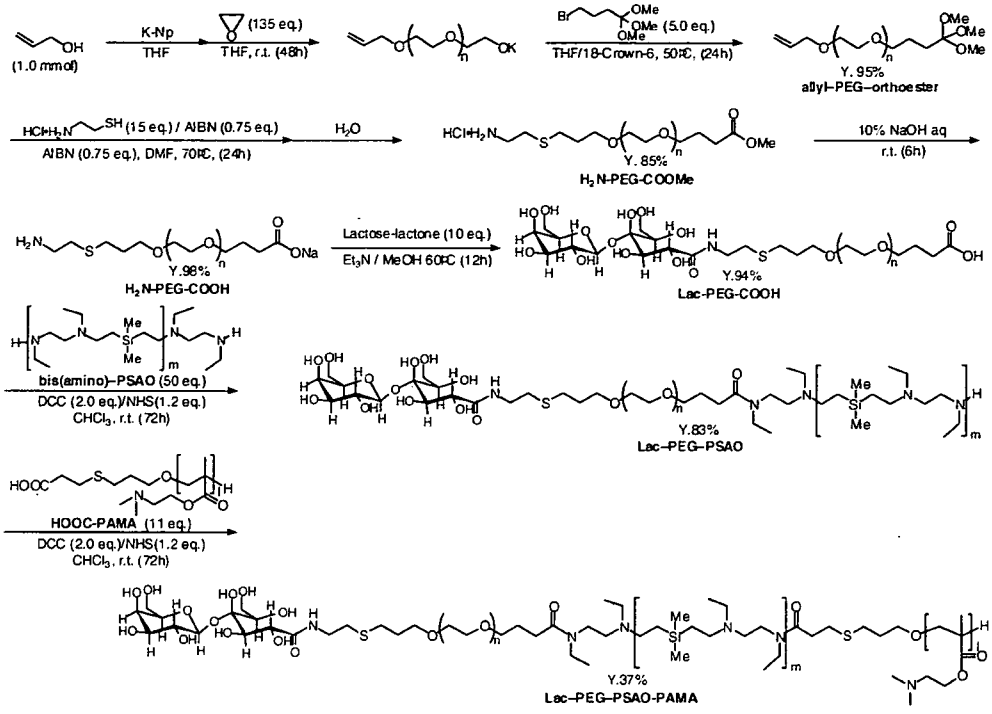

(Iwaki, Japan) and kept overnight at 37 °C in 5% CO_2 atmosphere. The Lac-PEG-PSAO-PAMA/pDNA and the Lac-PEG-PAMA/pDNA polyplex micelles (N/P = 3) containing FITC-labeled pDNA were added at a pDNA concentration of 30 μg/mL and incubated at 37 °C in 5% CO_2 atmosphere in the presence of Lysotraker Red DND-99 (50 nM) for 30 and 120 min. The cells were washed with PBS three times and imaged directly in the cell culture medium using an Olympus IX81 equipped with a confocal IX2-DSU system and an appropriate filter.

Transfection to HuH-7 Cells. HuH-7 cells were plated in a 24-well plate (5×10^4 cells/well) to reach about 50% confluence after 24 h at transfection, and the medium was then changed to fresh DMEM with 10% FBS (225 μL/well). For each well, the polyplex micelles or B-PEI/pDNA polyplexes at various N/P ratios (25 μL/well) were added with a pDNA concentration of 30 μg/mL. After 24 h incubation, the transfection medium was changed to fresh DMEM with 10% FBS, and the cells were further incubated for 24 h. For the preincubation study with serum, a medium containing 20% FBS was added to the solution of the polyplex micelles or B-PEI/pDNA polyplexes and incubated at 37 °C for 6 h prior to the transfection study. The cells were lysed, and the luciferase activity of the lysate was monitored with the a Luciferase Assay kit (Promega) and ARVOSX-1 (PerkinElmer). The results were expressed as light units per milligram of cell protein determined by a micro BCA assay kit (Pierce).

RESULTS AND DISCUSSION

Synthesis of Lactosylated Poly(ethylene glycol)-*block*-poly(silamine)-*block*-poly[2-(*N,N*-dimethlyamino)ethyl methacrylate] Triblock Copolymer. A synthetic route to lactosylated poly(ethylene glycol)-*block*-poly(silamine)-*block*-poy[2-(*N,N*-dimethlyamino)ethyl methacrylate] (Lac-PEG-PSAO-PAMA) triblock copolymer is shown in Scheme 1. A heterobifunctional PEG bearing an allyl group at the α-end and an ortho ester group at the ω-end (allyl-PEG-ortho ester) was synthesized via the anionic ring-opening polymerization of ethylene oxide using the allyl alcohol /potassium-naphthalene initiator system, followed by termination with trimethyl 4-bromoorthobutyrate in the presence of 18-Crown-6. The radical addition of 2-aminoethanethiol hydrochloride to the allyl-PEG-ortho ester quantitatively afforded an amine-PEG-methoxycarbonyl (H_2N-PEG-COOMe). Conversion of the ortho ester group into a methoxycarbonyl group (COOMe) occurred due to the hydrolysis of the ortho ester group during the purification (dialysis) process. The H_2N-PEG-COOMe was then converted into an amine-PEG-carboxylic acid (H_2N-PEG-COOH) by hydrolysis with 10% NaOHaq. The SEC (data not shown), ^{1}H NMR, and MALDI-TOF MS analyses (see Supporting Information) revealed that the determined molecular weight of the H_2N-PEG-COOH (SEC: M_n = 6200, M_w/M_n = 1.04, TOF-MS: M_n = 6190, M_w/M_n = 1.03) agrees well with the calculated value (calcd. M_n = 6130), and an amino group and carboxylic acid group were quantitatively introduced into the α-end and ω-end of PEG, respectively, to confirm the successful synthesis of allyl-PEG-ortho ester and H_2N-PEG-COOMe. The introduction of a lactose group to the amine end of H_2N-PEG-COOH was performed by reaction with an excess amount of lactose-lactone (*33*). In the ^{1}H NMR spectrum of Lac-PEG-COOH, the degree of lactose functionality was determined to be 72% (see Supporting Information).

To obtain the lactosylated PEG-PSAO block copolymer, bis(amino)-PSAO (M_n = 1550, the degree of polymerization (DP) = 6) was prepared as reported previously by the anionic polyaddition of dimethyldivinylsilane with *N,N'*-diethylethylenediamine in the presence of a catalytic amount of *n*-BuLi in THF at 60 °C (*24*–*29*). The conjugation of the Lac-PEG-COOH with bis(amino)-PSAO was performed by activating the terminal carboxylic acid of Lac-PEG-COOH using dicyclohexylcarbodiimide (DCC) and *N*-hydroxysuccinimide (NHS). A large excess (50 equiv) of the bis(amino)-PSAO was used to suppress the formation of triblock coplymer viz., Lac-PEG-PSAO-PEG-Lac. After the conjugation reaction, unconjugated bis(amino)-PSAO and other chemicals were removed by precipitation into Et_2O. Figures 3c and 4a, respectively, show the SEC chromatogram and ^{1}H NMR spectrum of the Lac-PEG-PSAO block

Table 1. Diameter (d), PDI (μ_2/Γ^2), and Zeta-Potential (ζ) of the Lac-PEG-PSAO-PAMA/pDNA, Lac-PEG-PAMA/pDNA, and Lac-PEG-PSAO/pDNA Polyplex Micelles Prepared at Various N/P Ratios

	Lac-PEG-PSAO−PAM A polyplex micelles		Lac-PEG-PAMA polyplex micelles		Lac-PEG-PSAO polyplex micelles	
N/P ratio	DLS[a] d (nm) /PDI (μ_2/Γ^2)	zeta-potential[b] (mV)	DLS[a] d (nm)/ PDI (μ_2/Γ^2)	zeta-potential[b] (mV)	DLS[a] d (nm)/ PDI (μ_2/Γ^2)	zeta-potential[b] (mV)
1	200.3/0.23	−4.3	196.5/0.24	−3.8	178.9/0.24	−5.8
2	175.4/0.23	+3.6	180.9/0.22	+3.8	166.6/0.20	−1.2
3	149.1/0.14	+4.7	147.0/0.14	+4.6	157.0/0.17	+0.6
4	147.2/0.17	+5.3	141.5/0.17	+4.8	163.4/0.22	+1.7
5	147.4/0.13	+5.1	140.0/0.19	+4.7	140.1/0.12	+2.3
7	146.8/0.18	+5.5	141.6/0.14	+5.0	144.7/0.19	+2.5
10	145.5/0.18	+5.4	136.1/0.12	+4.8	145.2/0.17	+2.4

[a] Conditions for DLS measurements: detection angle, 90°; solvent, 10 mM Tris-HCl, pH 7.4, including 0.15 M NaCl; temperature, 37 °C. [b] Conditions for zeta-potential measurements: solvent, 10 mM Tris-HCl, pH 7.4; temperature, 25 °C.

copolymer with assignments. As seen in the SEC chromatograms (Figure 3), Lac-PEG-PSAO (Figure 3c) gave a unimodal peak at a high molecular weight position (i.e., shorter elution time) compared to the Lac-PEG-COOH (M_n = 6300, M_w/M_n = 1.05, Figure 3a) and bis(amino)-PSAO (M_n = 1550, M_w/M_n = 2.01, Figure 3b). Note that the unreacted Lac-PEG-COOH and bis(amino)-PSAO were not observed in the SEC chromatogram (Figure 3c) of the Lac-PEG-PSAO (obsd. M_n = 7150, M_w/M_n = 1.15, calcd. M_n = 7850). In the ^{1}H NMR spectrum (Figure 4a), the peaks corresponding to both of the PEG and PSAO segments were clearly observed, consistent with the formation of a diblock copolymer. Note that the peaks corresponding to the terminal lactose moiety were also observed at δ 4.0−5.3 ppm in the ^{1}H NMR spectrum in DMSO-d_6. From the integral ratio between the PEG-backbone protons (3.7 ppm -OCH_2CH_2-) and the methyl protons of PSAO segment (0.1 ppm, $SiMe_2$), the DP of the PSAO segment in the block copolymer was calculated to be 5.67, which is in good accordance with that of the starting bis(amino)-PSAO (DP = 6).

To obtain the Lac-PEG-PSAO-PAMA triblock copolymer, the conjugation of the Lac-PEG-PSAO diblock copolymer and HOOC-PAMA was performed in a manner similar to the conjugation of Lac-PEG-COOH and bis(amino)-PSAO. After the conjugation reaction, unconjugated HOOC-PAMA and other chemicals were removed by precipitation into cold 2-propanol, followed by centrifugation. Figures 3e and 4b, respectively, show the SEC chromatogram and ^{1}H NMR spectrum of the Lac-PEG-PSAO-PAMA triblock copolymer with assignments. The Lac-PEG-PSAO-PAMA (Figure 3e, M_n = 10850, M_w/M_n = 1.29, calcd. M_n = 13450) had a shorter elution time compared to the Lac-PEG-PSAO (M_n = 7170, M_w/M_n = 1.15, Figure 3c) and HOOC-PAMA (M_n = 5670, M_w/M_n = 1.50, DP = 35, Figure 3d), indicating an increased molecular weight due to the formation of the triblock polymer. Nevertheless, a slight portion of unreacted Lac-PEG-PSAO and/or HOOC-PAMA seems to still remain (about 10%) in the sample as indicated by the small accompanying peak appearing after the main fraction (Figure 3e). In thethe ^{1}H NMR spectrum (Figure 4b), the peaks corresponding to the PEG, PSAO, and PAMA segments were clearly observed, suggesting the formation of a triblock copolymer. From the integral ratio between the PEG-backbone protons (3.7 ppm -OCH_2CH_2-) and methylene protons of the PAMA segment (4.08 ppm, -COOCH_2CH_2N(CH_3)$_2$), the DP of the PAMA segment was calculated to be 31.3 (DP of starting PAMA = 35). This result indicates that the purity of the triblock copolymer was 89%.

Furthermore, Lac-PEG-PSAO (M_{nPEG} = 6300, DP_{PSAO} = 6, number of amino groups = 12) and Lac-PEG-PAMA (M_{nPEG} = 6300, DP_{PAMA} = 55, number of amino groups = 55) diblock copolymers were prepared in a similar manner as the controls for the Lac-PEG-PSAO-PAMA (M_{nPEG} = 6300, DP_{PSAO} = 6, DP_{PAMA} = 35, total number of amino groups = 47).

Physicochemical Characterization of Polyplex Micelles. The obtained triblock (Lac-PEG-PSAO-PAMA) and diblock (Lac-PEG-PAMA and Lac-PEG-PSAO) copolymers form polyplex micelles through the mixing with pDNA based on electrostatic interaction. The size and surface charge of the polyplex micelles (Lac-PEG-PSAO-PAMA/pDNA, Lac-PEG-PAMA/pDNA, and Lac-PEG-PSAO/pDNA) was respectively evaluated by dynamic light scattering (DLS) and Laser-Doppler electrophoresis measurements at various N/P ratios, as summarized in Table 1. In the DLS measurements, the diameter (d) and polydipersity index (PDI; μ_2/Γ^2) of all the polyplex micelles decreased with increasing N/P ratios and reached plateau values of ca. 150 nm and 0.2, respectively, at an N/P ratio higher than 5. Concomitantly, as the N/P ratios increased, the zeta-potential (ζ) of all the polyplex micelles gradually shifted from a negative value (ζ < 0) to a positive value (ζ > 0). Nevertheless, the zeta-potential of all the polyplex micelles retained only a slightly positive value (ζ = +5 mV) even when the N/P ratio was increased to 10, suggesting the formation of a PEG corona surrounding the PIC core. These phenomena are consistent with the DNA condensation (coil-globule transition) upon complexation with the polycation segment in the block copolymers (*5*, *9*, *10*). It should also be noted that the N/P ratio to induce complete DNA condensation substantially shifted to a higher value from a stoichiometric mixing ratio (N/P = 1). A similar tendency was observed for the polyplex micelle from the PEG-PAMA block copolymer and pDNA (*4*).

To further clarify the behavior of DNA condensation, the quenching of the fluorescence intensity of the DNA intercalating dye, EtBr, was observed under physiological conditions for all of the polyplex micelles. Note that cationic EtBr is excluded from the DNA minor groove with the progress of the charge neutralization and the subsequent condensation of DNA due to the interaction with polycations, and therefore, this characteristic of EtBr is frequently utilized to estimate the degree of DNA condensation through complexation with a polycation. The profiles are shown in Figure 5a. In line with a trend in the hydrodynamic diameter and zeta-potential variations as shown in Table 1, the fluorescence intensity of EtBr decreased with increasing N/P ratios for all of the polyplex micelles, and the quenching of the fluorescence still continued even in the region of N/P > 1, suggesting that DNA condensation was not completely finished at the stoichiometric mixing ratio (N/P = 1) and that a nonstoichiometric complex may form in the range of N/P > 1. It should be noted that the amino groups of both PAMA and PSAO segments are incompletely protonated at physiological pH (= 7.4) because of their relatively lowered pKa values (PAMA: pK_a = 7.2, and PSAO: pK_{a1} = 8.6, pK_{a2} = 5.8). This may be a reason for the shift of the DNA-condensation point from a stoichiometric mixing ratio (N/P = 1). It should also be noted that a 35% decrease in fluorescence intensity compared to the initial value was observed for Lac-PEG-PSAO, whereas a decrease is more significant (50~55%)

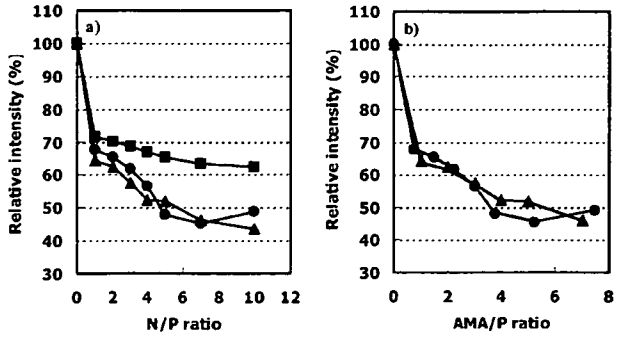

Figure 5. Ethidium bromide (EtBr) exclusion assay for the Lac-PEG-PSAO-PAMA/pDNA (circle), Lac-PEG-PAMA/pDNA (triangle), and Lac-PEG-PSAO/pDNA (square) systems. (a) Change in relative fluorescence intensity with the N/P ratio. (b) Change in relative fluorescence intensity with the AMA/P unit ratio ([amino groups in the PAMA segment]/[phosphate group in the pDNA]) (solvent, 10 mM Tris-HCl buffer including 0.15 M NaCl (pH 7.4); temperature, 37 °C).

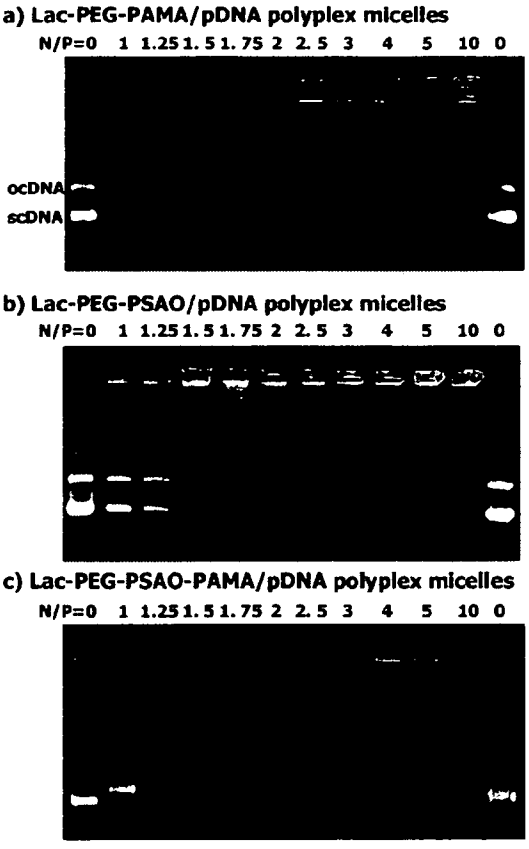

Figure 6. Agarose gel electrophoresis of the (a) Lac-PEG-PAMA/pDNA, (b) Lac-PEG-PSAO/pDNA, and (c) Lac-PEG-PSAO-PAMA/pDNA polyplex micelles prepared at various N/P ratios.

for Lac-PEG-PAMA and Lac-PEG-PSAO-PAMA, and their fluorescence intensities of Lac-PEG-PSAO-PAMA were almost identical when the N/P ratio was converted to the AMA/P ([amino groups in the PAMA segment]/[phosphate group in the pDNA]) unit ratio (Figure 5b), suggesting that the PAMA segment may preferentially take part in the complexation with DNA in the Lac-PEG-PSAO-PAMA/pDNA system, bearing the PSAO segment in the free form.

To evaluate the stability of the polyplex micelle, an agarose gel retardation assay at various N/P ratios was carried out. As shown in Figure 6, two topologically different forms of pDNA, i.e., supercoiled (scDNA) and open circular (ocDNA), were clearly observed in the absence of the block copolymer (at N/P = 0). In the cases of Lac-PEG-PSAO-PAMA/pDNA and Lac-PEG-PAMA/pDNA polyplex micelles, pDNA migration was completely retarded at an N/P ratio ≥ 1.5 (Figure 6a,c). Alternatively, a higher N/P ratio (≥ 3) was required for the complete retardation of pDNA for Lac-PEG-PSAO/pDNA polyplex micelles (Figure 6b). Presumably, excess cationic component may be needed for the Lac-PEG-PSAO block copolymer with a shorter cationic segment to induce effective DNA stabilization.

The polyplex micelle from Lac-PEG-PSAO-PAMA and pDNA was characterized by ^{1}H NMR spectroscopy in D_2O containing 0.15 M NaCl at pD = 7.4. Figure 7f shows the ^{1}H NMR spectrum of the polyplex micelle prepared at N/P = 3, where the residual molar ratio of the protonated PAMA segment in the block copolymer, calculated from the pK_a value, to the phosphate groups in pDNA is estimated to be unity at physiological pH (= 7.4). Note that the DNA condensation process was almost completed at N/P = 3, as shown in Table 1. Obviously, the peaks from the PAMA segment, which were clearly observed in the spectrum of the free polymers (Figure 7c), nearly disappeared upon complexation with pDNA (Figure 7f), whereas the peaks from the PSAO segment were still clearly observed in the spectrum. The selective disappearance of PAMA peaks upon complexation strongly suggests that the PAMA segment predominantly forms a PIC with pDNA to cause significant peak broadening. On the other hand, observation of the peaks from the PSAO segment even in the spectrum of the polyplex micelle suggests the presence of the uncomplexed PSAO fraction. Eventually, these results are consistent with the formation of the three-layered structure of the polyplex micelle with a PAMA/pDNA PIC core, a free PSAO inner shell, and a lactosylated PEG outer shell, as illustrated in Figure 2. In sharp contrast to the Lac-PEG PSAO-PAMA/pDNA system, peaks corresponding to polyamine segments (PAMA and PSAO) completely disappeared in the NMR spectra of the polyplex micelles from diblock copolymers (Lac-PEG-PAMA/pDNA (Figure 7d) and Lac-PEG-PSAO/pDNA (Figure 7e)) due to the limited molecular motion in the complex form.

pH Response of the Polyplex Micelles. To estimate the effect of the environmental pH on the hydrodynamic diameter of the polyplex micelles, the Lac-PEG-PSAO-PAMA/pDNA, Lac-PEG-PSAO/pDNA, and Lac-PEG-PAMA/pDNA polyplex micelles were prepared in 0.15 M NaClaq (pH 7.4) at N/P = 3. By decreasing the pH from 7.4 to 4.0, the diameter (d) of the Lac-PEG-PSAO-PAMA/pDNA and Lac-PEG-PSAO/pDNA polyplex micelles proportionally increases with a unimodal distribution ($\mu_2/\Gamma^2 < 0.25$), reaching a 2.7-times larger hydrodynamic volume at pH 4.0 compared to that at pH 7.4, as shown in Figure 8. On the contrary, there was negligible change in the hydrodynamic diameter of the Lac-PEG-PAMA/pDNA polyplex micelle with decreasing pH from 7.4 to 4.0. This pH-induced size variation observed for the system containing the PSAO segment is most likely to be related to the conformational changes in the PSAO chain due to progressive protonation with decreasing pH. In the ^{1}H NMR spectrum of the Lac-PEG-PAMA/pDNA polyplex micelle (N/P = 3) at pD = 4.0, the peaks from the PAMA segment almost disappeared, indicating that pDNA was still condensed even at pD = 4.0 by the PAMA segment (see Supporting Information). Furthermore, the ^{1}H NMR spectrum of the Lac-PEG-PSAO-PAMA/pDNA polyplex micelle at pD = 4.0 shows only the peaks assigned to the PSAO segment along with the PEG segment, suggesting the three-layered structure even at pD = 4.0 (see Supporting Information). This result supports the plausible scheme that the globule-to-rod conformational changes in the uncomplexed PSAO segment in the three-layered Lac-PEG-PSAO-PAMA/pDNA polyplex